Appendix I

Corrected Emission Spectra

A relatively limited number of corrected emission spectra are available. In this Appendix we include the well-documented corrected spectra. It is not possible to state which are the "most correct." Corrected spectra can be interchanged from photons per wavenumber interval $I(\bar{\nu})$ to photons per wavelength interval $I(\lambda)$ using $I(\lambda) = I(\bar{\nu})\lambda^{-2}$, followed by normalization of the peak intensity to unity. Most of the compounds listed below satisfy the suggested criteria for emission spectral standards, which are as follows:

1. Broad wavelength emission with no fine structure
2. Chemically stable, easily available and purified
3. High quantum yield
4. Emission spectrum independent of excitation wavelength
5. Completely depolarized emission.

1. EMISSION SPECTRA STANDARDS FROM 300 TO 800 NM

Corrected emission spectra on the wavelength scale were reported for six readily available fluorophores in neat solvents (Table I.1). The emission spectra of these standards overlap, providing complete coverage from 300 to 800 nm. For convenience the numerical values of the emission spectra are given in Table I.2. The values are plotted in Figure I.1, and the chemical structures are given in Figure I.2. These correct spectra cover almost all needed wavelengths. It is recommended that these spectra be adopted as the accepted standards for determination of instrument corrections factors and for calculation of corrected emission spectra.

2. β-CARBOLINE DERIVATIVES AS FLUORESCENCE STANDARDS

Corrected emission spectra of the carboline derivatives shown in Figure I.3 and I.4 were published.[2] All compounds were measured in 0.1 N H_2SO_4, except for 2-methylharmine, which was measured in 0.01 N H_2SO_4, 25°C. Corrected emission spectra were reported in graphical form (Figure I.3) and in numerical form (Table I.3). Quantum yields and lifetimes were also reported (Table I.4). Quantum yields were determined relative to quinine sulfate in 1.0

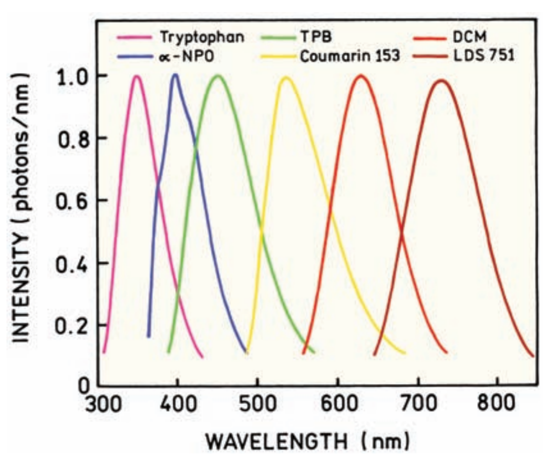

Figure I.1. Corrected emission spectra of six standards from [1]. From left to right the spectra are for tryptophan, α-NPO, TPB, coumarin, DCM, and LDS 751.

Table I.1. Properties of the Emission Intensity Standards*

Probe	CAS	Solvent	Excitation	Emission range
Tryptophan	54-12-6	Water	265	310–428
α-NPO	846-63-9	Methanol	315	364–486
TPB	1450-63-1	Cyiohexane	340	390–570
Coumarin 153	53518-18-6	Methanol	400	486–678
DCM	51325-91-8	Methanol	460	556–736
LDS 751	N/A	Methanol	550	646–844

*CAS number (Chemical Abstract Service registry number) provides a unique identification for each fluorophore. The excitation wavelength and emission range is reported in nm. LDS-751 is a proprietary material of Exciton Inc. (Dayton, OH) and is similar to Styrl 8. Coumarin 153 is also referred to as Coumarin 540A (Exciton). From [1].

Table I.2. Normalized Emission Intensities for Each Emission Standard
(emission wavelength is reported in nm and intensity given in photons/nm)

Tryptophan		NPO		TPB		Coumarine 153		DCM		LDS 751	
nm	int.	nm	int.	nm	int.	nm	int.	nm	int.	nm	int.
310	0.111	364	0.162	390	0.11	486	0.118	556	0.1	646	0.101
312	0.149	366	0.247	392	0.137	488	0.142	558	0.115	648	0.114
314	0.194	368	0.342	394	0.167	490	0.169	560	0.132	650	0.128
316	0.242	370	0.433	396	0.199	492	0.2	562	0.148	652	0.143
318	0.299	372	0.509	398	0.235	494	0.235	564	0.168	654	0.159
320	0.357	374	0.571	400	0.271	496	0.274	566	0.19	656	0.177
322	0.417	376	0.618	402	0.31	498	0.315	568	0.214	658	0.196
324	0.485	378	0.656	404	0.35	500	0.36	570	0.238	660	0.216
326	0.547	380	0.69	406	0.393	502	0.407	572	0.266	662	0.238
328	0.611	382	0.725	408	0.436	504	0.458	574	0.303	664	0.26
330	0.675	384	0.764	410	0.478	506	0.509	576	0.331	666	0.284
332	0.727	386	0.813	412	0.525	508	0.56	578	0.353	668	0.308
334	0.771	388	0.864	414	0.571	510	0.613	580	0.38	670	0.334
336	0.814	390	0.915	416	0.62	512	0.665	582	0.412	672	0.361
338	0.86	392	0.959	418	0.663	514	0.715	584	0.444	674	0.388
340	0.906	394	0.988	420	0.699	516	0.762	586	0.478	676	0.416
342	0.928	396	0.999	422	0.735	518	0.806	588	0.513	678	0.445
344	0.957	398	1	424	0.773	520	0.847	590	0.548	680	0.474
346	0.972	400	0.991	426	0.805	522	0.882	592	0.584	682	0.504
348	0.996	402	0.978	428	0.834	524	0.914	594	0.62	684	0.534
350	1	404	0.959	430	0.864	526	0.941	596	0.659	686	0.564
352	0.999	406	0.94	432	0.887	528	0.962	598	0.696	688	0.594
354	0.987	408	0.921	434	0.91	530	0.979	600	0.732	690	0.624
356	0.972	410	0.901	436	0.931	532	0.99	602	0.763	692	0.653
358	0.946	412	0.886	438	0.951	534	0.997	604	0.79	694	0.682
360	0.922	414	0.87	440	0.963	536	1	606	0.818	696	0.711
362	0.892	416	0.855	442	0.976	538	1	608	0.842	698	0.738
364	0.866	418	0.835	444	0.985	540	0.996	610	0.869	700	0.765
366	0.837	420	0.803	446	0.991	542	0.991	612	0.893	702	0.791
368	0.798	422	0.773	448	0.998	544	0.981	614	0.915	704	0.815
370	0.768	424	0.743	450	0.999	346	0.97	616	0.934	706	0.839
372	0.728	426	0.708	452	1	548	0.958	618	0.953	708	0.86
374	0.697	428	0.676	454	0.993	550	0.944	620	0.968	710	0.881
376	0.663	430	0.644	456	0.987	552	0.929	622	0.98	712	0.899
378	0.627	432	0.611	458	0.981	554	0.914	624	0.989	714	0.916
380	0.592	434	0.58	460	0.969	556	0.898	626	0.995	716	0.931
382	0.558	436	0.55	462	0.957	558	0.884	628	0.999	718	0.946
384	0.523	438	0.521	464	0.944	560	0.867	630	1	720	0.956
386	0.492	440	0.494	466	0.931	562	0.852	632	0.998	722	0.965

[continued]

Table I.2, cont'd

388	0.461	442	0.467	468	0.915	564	0.835	634	0.994	724	0.973
390	0.43	444	0.441	470	0.896	566	0.818	636	0.986	726	0.978
392	0.404	446	0.418	472	0.879	568	0.801	638	0.978	728	0.982
394	0.375	448	0.394	474	0.856	570	0.785	640	0.964	730	0.984
396	0.348	450	0.371	476	0.835	572	0.768	642	0.952	732	0.983
398	0.323	452	0.349	478	0.816	574	0.75	644	0.938	734	0.982
400	0.299	454	0.326	480	0.796	576	0.729	646	0.923	736	0.977
402	0.279	456	0.306	482	0.775	578	0.712	648	0.904	738	0.971
404	0.259	458	0.285	484	0.752	580	0.69	650	0.886	740	0.963
406	0.239	460	0.266	486	0.727	582	0.672	652	0.867	742	0.954
408	0.222	462	0.248	488	0.706	584	0.653	654	0.843	744	0.943
410	0.204	464	0.232	490	0.68	586	0.634	656	0.821	746	0.931
412	0.19	466	0.216	492	0.657	588	0.615	658	0.795	748	0.917
414	0.176	468	0.201	494	0.633	590	0.596	660	0.771	750	0.902
416	0.163	470	0.187	496	0.609	592	0.576	662	0.745	752	0.885
418	0.151	472	0.174	498	0.586	594	0.557	664	0.718	754	0.868
420	0.139	474	0.162	500	0.564	596	0.538	666	0.694	756	0.849
422	0.128	476	0.151	502	0.542	598	0.518	668	0.666	758	0.83
424	0.118	478	0.14	504	0.521	600	0.501	670	0.639	760	0.81
426	0.109	480	0.131	506	0.499	602	0.483	672	0.613	762	0.789
428	0.101	482	0.122	508	0.476	604	0.465	674	0.586	764	0.767
		484	0.113	510	0.456	606	0.447	676	0.559	766	0.745
		486	0.105	512	0.437	608	0.43	678	0.534	768	0.722
				514	0.419	610	0.414	680	0.509	770	0.699
				516	0.4	612	0.398	682	0.485	772	0.676
				518	0.382	614	0.383	684	0.46	774	0.653
				520	0.364	616	0.368	686	0.431	776	0.63
				522	0.348	618	0.355	688	0.407	778	0.606
				524	0.332	620	0.341	690	0.391	780	0.583
				526	0.318	622	0.328	692	0.371	782	0.56
				528	0.302	624	0.315	694	0.355	784	0.537
				530	0.289	626	0.303	696	0.336	786	0.514
				532	0.274	628	0.292	698	0.319	788	0.492
				534	0.261	630	0.28	700	0.302	790	0.47
				536	0.249	632	0.269	702	0.284	792	0.449
				538	0.237	634	0.258	704	0.268	794	0.428
				540	0.226	636	0.248	706	0.254	796	0.407
				542	0.215	638	0.239	708	0.239	798	0.387
				544	0.205	640	0.229	710	0.225	800	0.368
				546	0.194	642	0.219	712	0.212	802	0.349
				548	0.184	644	0.211	714	0.199	804	0.331
				550	0.175	646	0.204	716	0.188	806	0.313
				552	0.166	648	0.195	718	0.177	808	0.296
				554	0.158	650	0.188	720	0.166	810	0.28
				556	0.15	652	0.18	722	0.156	812	0.264
				558	0.143	654	0.173	724	0.147	814	0.249
				560	0-135	656	0.166	726	0.138	816	0.234
				562	0.129	658	0.159	728	0.131	818	0.221
				564	0.122	660	0.152	730	0.123	820	0.207
				566	0.116	662	0.146	732	0.116	822	0.195
				568	0.11	664	0.14	734	0.109	824	0.183
				570	0.105	666	0.134	736	0.103	826	0.171
						668	0.129			828	0.16
						670	0.124			830	0.15
						672	0.118			832	0.14
						674	0.113			834	0.131
						676	0.108			836	0.122
						678	0.104			838	0.114
										840	0.106
										842	0.099
										844	0.092

Table I.3. Normalized and Corrected Fluorescence Spectra for Nor-harmane, Harmane, Harmine, 2-Methyl Harmine, and Harmaline in H_2SO_4 Aqueous Solutions (0.1 N H_2SO_4 for nor-harmane, harmane, harmine and 2-methyl harmine and 0.01 N for harmaline)*

Wave length (nm)	Nor-harmane or β-carboline	Harmane	Harmine	2-Methyl harmine	Harmaline
400			0.63		
405			0.76	0.53	
410			0.87	0.68	
415		0.56	0.93	0.78	
420		0.70	0.98	0.89	
425	0.54	0.81	1.00	0.95	
430	0.67	0.90	0.99	0.98	
433				1.00	
435	0.79	0.97	0.94	0.99	
440	0.90	1.00	0.97**	0.97	
445	0.96	0.98	0.80	0.90	
450	0.99	0.94	0.73	0.84	
454	1.00				
455	0.99	0.88	0.64	0.76	
460	0.98	0.82	0.54	0.66	0.48
465	0.96	0.76	0.48	0.58	0.59
470	0.93	0.69		0.52	0.69
475	0.87	0.61		0.44	0.78
480	0.83	0.56			0.86
485	0.78	0.50			0.92
490	0.73				0.96
495	0.67				0.98
498					1.00
500	0.61				0.99
505	0.54				0.97
510					0.96
515					0.92
520					0.89
525					0.83
530					0.77
535					0.74
540					0.71
550					0.59
560					0.49

*From [2].
**This number is in question.

Table I.4. Quantum Yields and Lifetimes of the β-Carboline Standards[a] (from [2])

Compound	Quantum yield	Lifetime (ns)
Nor-harmane	0.58 ± 0.02	21.2
Harmane	0.83 ± 0.03	20.0 ± 0.5
Harmine	0.45 ± 0.03	6.6 ± 0.2
2-Methylharmine	0.45 ± 0.03	6.5 ± 0.2
Harmaline	0.32 ± 0.02	5.3 ± 0.2

[a]Same conditions as in Table I.3.

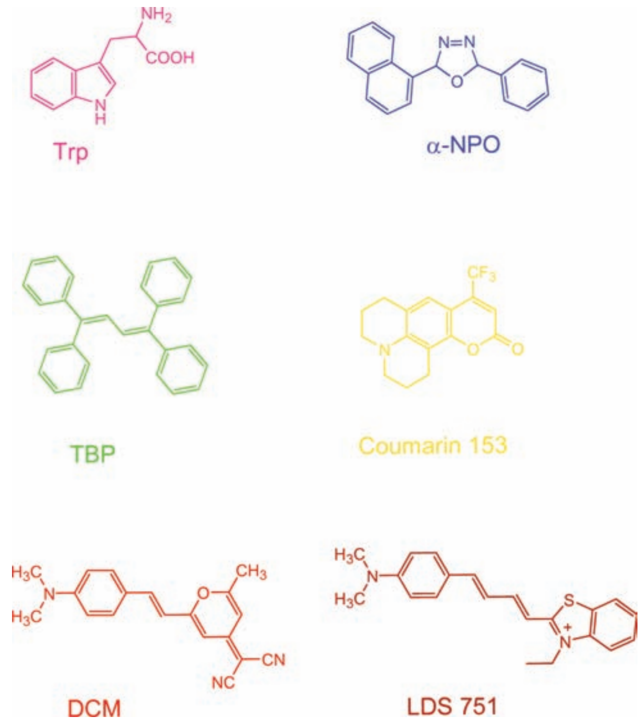

Figure I.2. Chemical structure of the emission spectra standards.

N H_2SO_4, with $Q = 0.546$. Corrected spectra are in relative quanta per wavelength interval. A second corrected emission spectrum of nor-harmane (β-carboline) was also reported (Table I.5).[3] The spectral properties of β-carboline are similar to quinine sulfate. While the polarization of the β-carboline standards was not measured, these values are likely to be near zero given the lifetimes near 20 ns (Table I.4).

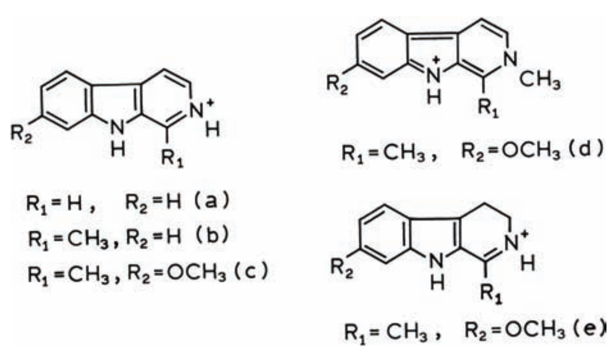

Figure I.3. β-Carboline standards. Cationic species structures: (a) β-carboline or nor-harmane, (b) harmane, (c) harmine, (d) 2-methyl harmine, and (e) harmaline. Revised from [2]. Copyright © 1992, with permission from Elsevier Science.

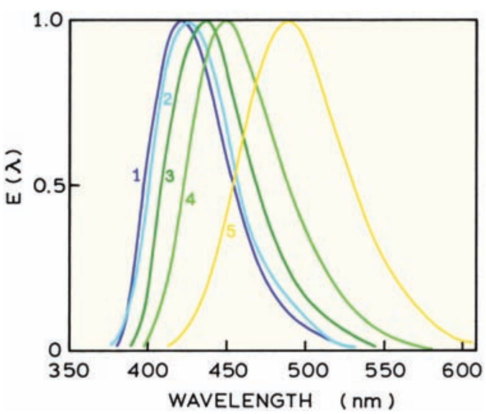

Figure I.4. Corrected and normalized fluorescence spectra for some β-carboline derivatives: (1) harmine 0.1 N H_2SO_4; (2) 2-methyl harmine 0.1 N H_2SO_4; (3) harmane 0.1 N H_2SO_4; (4) nor-harmane 0.1 N H_2SO_4; (5) harmaline 0.01 N H_2SO_4. Revised from [2]. Copyright © 1992, with permission from Elsevier Science.

Table I.5. Corrected Emission Intensities for β-Carboline in 1.0 N H_2SO_4 at 25°C[a]

Wave-length (nm)	Corrected intensity	Wave-length (nm)	Corrected intensity
380	0.001	510	0.417
390	0.010	520	0.327
400	0.068	530	0.255
410	0.243	540	0.193
420	0.509	550	0.143
430	0.795	560	0.107
440	0.971	570	0.082
450	1.000	580	0.059
460	0.977	590	0.044
470	0.912	600	0.034
480	0.810	610	0.025
490	0.687	620	0.019
500	0.540	630	0.011

[a]Excitation at 360 nm. From [3].

3. CORRECTED EMISSION SPECTRA OF 9,10-DIPHENYLANTHRACENE, QUININE, AND FLUORESCEIN

Corrected spectra in quanta per wavelength interval *I*(λ) were published for these three compounds[4] (Figure I.5 and Table I.6). The emission spectrum for quinine was found to be at somewhat shorter wavelengths than that published by Melhuish.[5]

4. LONG-WAVELENGTH STANDARDS

Corrected emission spectra in relative quanta per wavelength interval were reported[4] for quinine sulfate (QS), 3-aminophthalimide (3-APT), and N,N-dimethylamino-m-nitrobenzene (N,N-DMAMB). Chemical structures are shown in Figure I.6. These standards are useful because they extend the wavelength range to 750 nm (Figure I.7).

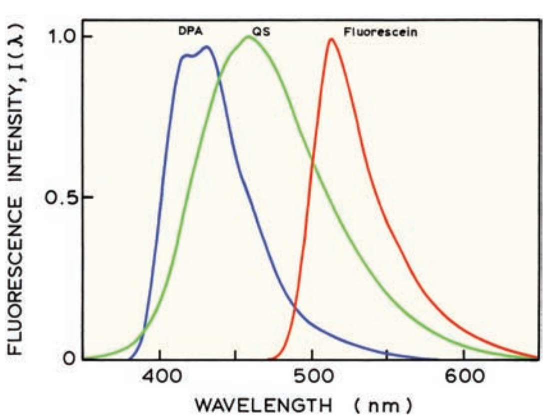

Figure I.5. Corrected emission spectra in relative photons per wavelength interval (*I*(λ)) for 9,10-diphenylanthracene, quinine sulfate, and fluorescein. From [4].

Table I.6. Corrected Emission Spectra in Relative Quanta per Wavelength Interval (from [4])

Quinine sulfate[a] λ (nm)	*I*(λ)	Fluorescein[b] λ (nm)	*I*(λ)	DPA[c] λ (nm)	*I* (λ)
310	0	470	0	380	0
350	4	480	7	390	39
380	18	490	151	400	423
400	151	495	360	412	993
410	316	500	567	422	914
420	538	505	795	432	1000
430	735	510	950	440	882
440	888	512	1000	450	607
445	935	515	985	460	489
450	965	520	933	470	346
455	990	525	833	480	222
457.2	1000	530	733	490	150
400	998	540	533	500	103
465	979	550	417	550	4
470	951	560	333	600	0
475	916	570	233		
480	871	580	167		
490	733	600	83		
500	616	620	42		
520	408	640	17		
550	171	650	8		
600	19	670	0		
650	3				
700	0				

[a]Quinine sulfate was in 1.0 N H_2SO_4, excitation at 346.5.
[b]Fluorescein (Uranine) was in 0.1 N NaOH, excitation at 322 nm.
[c]9,10-diphenylanthracene (DPA) was in benzene, excitation at 385 nm.

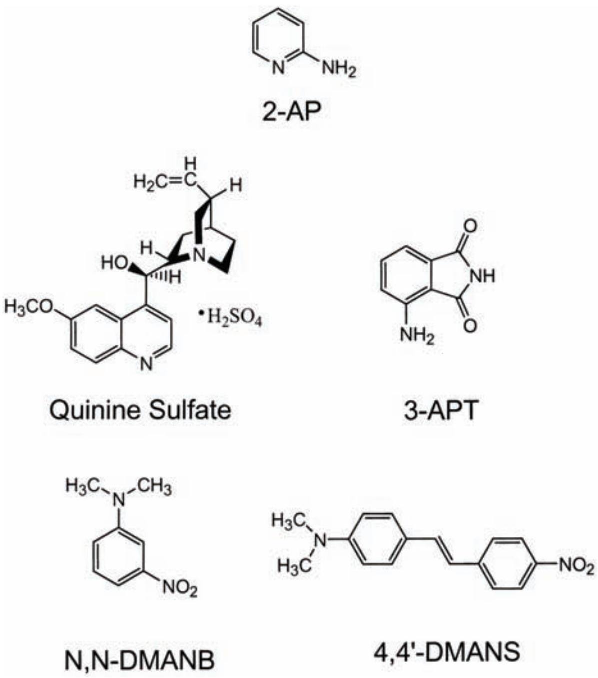

Figure I.6. Chemical structure of fluorophores used as spectral standards.

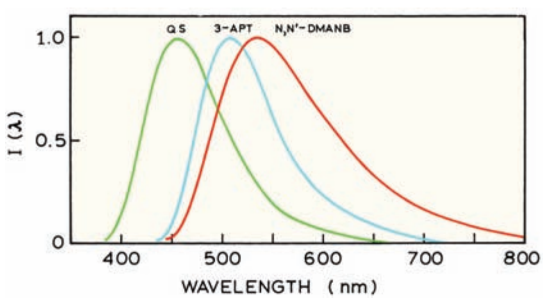

Figure I.7. Corrected emission spectra in relative quanta per wavelength interval ($I(\bar{\nu})$). The quinine sulfate (QS) was in 0.1 N H_2SO_4. 3-aminophthalamide (3-APT) was in 0.1 N H_2SO_4. N,N-dimethylamino-m-nitrobenzene (N,N-DMANB) was in 70% n-hexane, 30% benzene. Modified from [4].

The data were not reported in numerical form. These corrected emission spectra $I(\lambda)$ were in agreement with that reported earlier[6] in relative quanta per wavenumber ($I(\bar{\nu})$), following the appropriate transformation.

A more complete set of corrected spectra,[6,7] in $I(\bar{\nu})$ per wavenumber interval, are summarized numerically in Figure I.8 and Table I.7. These data contain an additional standard, 4-dimethylamino-4'-nitrostilbene (4,4'-DMANS), which extends the wavelength range to 940 nm. These spectra are plotted on the wavenumber scale in Figure I.8. For convenience the data were transformed to the wavelength scale, and are shown in Figure I.9 and Table I.8. In summarizing these corrected spectra we omitted β-naphthol, whose emission spectrum depends on pH and buffer concentration. Because these factors change its spectral shape, naphthol is not a good standard.

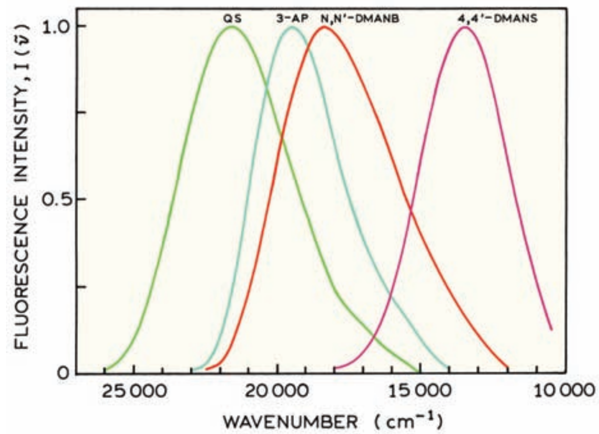

Figure I.8. Corrected emission spectra in relative quanta per wavenumber interval $I(\bar{\nu})$. See Table I.6 for additional details. Data from [6] and [7].

5. ULTRAVIOLET STANDARDS

2-aminopyridine (Figure I.10) has been suggested as a standard from 315 to 480 nm,[8,9] which covers most but not all of the wavelengths needed for tryptophan fluorescence

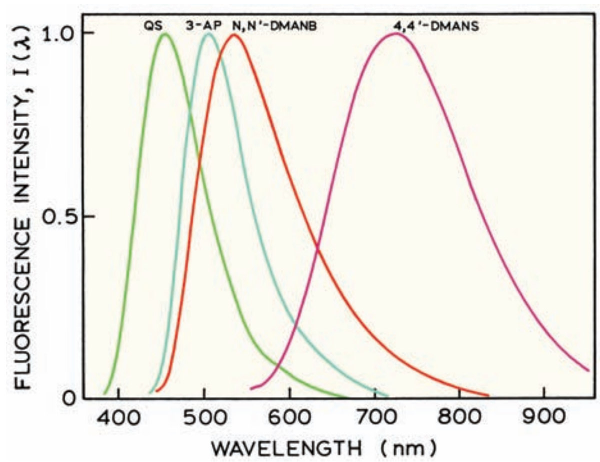

Figure I.9. Corrected emission spectra in relative quanta per wavelength interval $I(\lambda)$. See Table I.5 for additional details. Data from [6] and [7].

Table I.7. Corrected Emission Spectra in Relative Quanta per Wavenumber Interval

Quinine sulfate[b]		3-APT[c]		N,N'-DMANB[d]		4,4'-DMANS[e]	
$\bar{\nu}$(cm^{-1})	$I(\bar{\nu})$	$\bar{\nu}$ (cm^{-1})	$I(\bar{\nu})$	$\bar{\nu}$ (cm^{-1})	$I(\bar{\nu})$	$\bar{\nu}$ (cm^{-1})	$I(\bar{\nu})$
15.0	0	14.0	1.5	12.0	2.0	10.5	12.5
15.25	1.5	14.25	3.0	12.25	4.0	10.75	18.5
15.5	3.0	14.5	5.0	12.5	6.0	11.0	24.5
15.75	4.5	14.75	7.5	12.75	8.5	11.25	32.5
16.0	6.0	15.0	10.0	13.0	11.0	11.5	41.5
16.25	7.5	15.25	13.0	13.25	13.5	11.75	50.5
16.5	9.5	15.5	16.0	13.5	17.0	12.0	60.0
16.75	11.5	15.75	19.0	13.75	20.0	12.25	70.5
17.0	14.0	16.0	22.0	14.0	23.5	12.5	80.5
17.25	16.0	16.25	25.5	14.25	27.5	12.75	89.0
17.5	18.0	16.5	29.5	14.5	31.0	13.0	95.0
17.75	20.5	16.75	33.5	14.75	35.5	13.25	98.5
18.0	24.0	17.0	38.5	15.0	40.5	13.5	100.0
18.25	28.5	17.25	44.0	15.25	45.0	13.75	98.0
18.5	34.5	17.5	50.0	15.5	50.0	14.0	94.0
18.75	40.5	17.75	56.5	15.75	55.5	14.25	88.0
19.0	46.0	18.0	65.0	16.0	61.5	14.5	81.0
19.25	52.5	18.25	73.0	16.25	68.0	14.75	72.0
19.5	58.5	18.5	82.5	16.5	73.0	15.0	61.5
19.75	65.0	18.75	90.0	16.75	78.0	15.25	51.0
20.0	71.5	19.0	95.0	17.0	82.5	15.5	41.0
20.25	78.5	19.25	98.5	17.25	87.0	15.75	32.0
20.5	84.5	19.5	100.0	17.5	91.5	16.0	24.0
20.75	90.0	19.75	98.5	17.75	95.0	16.25	17.5
21.0	95.0	20.0	94.5	18.0	97.5	16.5	13.0
21.25	98.5	20.25	87.5	18.25	99.5	16.75	9.0
21.5	100.0	20.5	77.5	18.5	99.5	17.0	6.0
21.75	99.5	20.75	66.0	18.75	97.5	17.25	4.0
22.0	98.0	21.0	53.0	19.0	93.5	17.5	2.5
22.25	94.5	21.25	39.5	19.25	87.0	17.75	2.0
22.5	89.0	21.5	28.0	19.5	80.0	18.0	1.5
22.75	82.5	21.75	17.5	19.75	71.5		
23.0	74.0	22.0	11.0	20.0	61.0		
23.25	65.5	22.25	6.0	20.25	51.0		
23.5	55.5	22.5	3.0	20.5	41.5		
23.75	46.0	22.75	1.5	20.75	32.5		
24.0	37.5	23.0	1.0	21.0	23.5		
24.25	29.5			21.25	16.0		
24.5	21.0			21.5	10.5		
24.75	15.0			21.75	6.0		
25.0	10.5			22.0	3.0		
25.25	6.5			22.25	2.0		
25.5	4.0			22.5	1.5		
25.75	2.5						
26.0	1.0						
Max.		Max.		Max.		Max.	
21.6	100.0	19.5	100.0	18.4	100.0	13.5	100.0

[a]All listings are in 10^3 cm^{-1}, that is, 13.5 is 13,500 cm^{-1}.
[b]Quinine sulfate (10^{-3} M) in 0.1 N H_2SO_4, 20°C.
[c]3-aminophthalimide (5 x 10^{-4} M) in 0.1 N H_2SO_4, 20°C.
[d]N,N-dimethylamino-m-nitrobenzene (10^{-4} M) in 30% benzene, 70% n-hexane, 20°C.
[e]4-dimethylamino-4'-nitrostilbene in o-dichlorobenzene, 20°C.

Table I.8. Corrected Emission Spectra in Relative Quanta per Wavelength Interval[f]

Quinine sulfate[b]		3-APT[c]		N,N-DMANB[d]		4,4'-DMANS[e]	
λ (nm)[a]	*I*(λ)	λ (nm)	*I*(λ)	λ (nm)	*I*(λ)	λ (nm)	*I*(λ)
384.6	1.4	434.8	1.4	444.4	2.2	555.6	2.6
388.3	3.5	439.6	2.0	449.4	2.9	563.4	3.4
392.2	5.5	444.4	4.0	454.5	4.2	571.4	4.1
396.0	8.7	449.4	7.7	459.8	8.3	579.7	6.4
400.0	13.8	454.5	13.9	465.1	14.2	588.2	9.4
404.0	19.4	459.8	21.5	470.6	21.1	597.0	13.6
408.2	26.6	465.1	33.7	476.2	30.2	606.1	19.1
412.4	36.6	470.6	46.4	481.9	40.8	615.4	24.9
416.7	45.5	476.2	60.8	487.8	50.9	625.0	33.2
421.1	54.7	481.9	74.0	493.8	61.0	634.9	42.8
425.5	64.6	487.8	84.8	500.0	71.2	645.2	53.2
430.1	74.6	493.8	93.4	506.3	81.4	655.7	64.0
434.8	82.5	500.0	98.4	512.8	88.7	666.7	74.7
439.6	90.0	506.3	100.0	519.5	94.1	678.0	84.5
444.4	95.0	512.8	99.0	526.3	98.5	689.7	91.9
449.4	98.6	519.5	95.0	533.3	100.0	701.8	96.4
454.5	100.0	526.3	89.2	540.5	99.3	714.3	99.4
459.8	99.2	533.3	82.3	547.9	96.7	727.3	100.0
465.1	97.5	540.5	73.5	555.6	92.2	740.7	98.4
470.6	93.8	547.9	63.3	563.4	87.3	754.7	93.3
476.2	88.3	555.6	54.8	571.4	81.8	769.2	86.7
481.9	81.7	563.4	46.3	579.7	75.5	784.3	78.1
487.8	74.9	571.4	39.9	588.2	69.6	800.0	67.9
493.8	67.9	579.7	34.1	597.0	63.8	816.3	57.1
500.0	60.3	588.2	29.0	606.1	58.0	833.3	46.6
506.3	53.4	597.0	24.5	615.4	52.4	851.1	37.6
512.8	46.9	606.1	20.9	625.0	45.9	869.6	29.6
519.5	41.0	615.4	17.5	634.9	40.2	888.9	22.2
526.3	35.0	625.0	14.7	645.2	35.0	909.1	16.0
533.3	30.0	634.9	12.3	655.7	30.5	930.2	11.5
540.5	24.9	645.2	10.0	666.7	26.6	952.4	7.4
547.9	20.0	655.7	7.9	678.0	22.5		
555.6	16.4	666.7	5.9	689.7	19.0		
563.4	13.6	678.0	4.2	701.8	16.3		
571.4	11.6	689.7	2.7	714.3	13.4		
579.7	10.0	701.8	1.6	727.3	11.0		
588.2	8.5	714.3	0.8	740.7	9.0		
597.0	6.8			754.7	6.9		
606.1	5.5			769.2	5.4		
615.4	4.2			784.3	4.0		
625.0	3.2			800.0	2.7		
634.9	2.4			816.3	1.8		
645.2	1.5			833.3	0.8		
655.7	0.7						
666.7	0.0						

[a] Calculated from Table I.7.
[b] Quinine sulfate (10^{-3} M) in 0.1 N H_2SO_4, 20°C.
[c] 3-aminophthalimide (5×10^{-4} M) in 0.1 N H_2SO_4, 20°C.
[d] N,N'-dimethylamino-m-nitrobenzene (10^{-4} M) in 30% benzene, 70% m-heptane, 20°C
[e] 4-dimethylamino-4'-nitrostilbene in o-dichlorobenzene, 20°C.
[f] Calculated from Table I.7 using $I(\lambda) = \lambda^{-2} I(\bar{\nu})$, followed by normalization of the peak intensity to 100.

Table I.9. Corrected Emission Spectrum of 2-Aminopyridine[a]

$\bar{\nu}$ (cm^{-1})	$I(\bar{\nu})$	λ (nm)	$I(\lambda)$[b]
20,800	0.010	480.8	0.006
21,500	0.038	465.1	0.024
22,200	0.073	450.5	0.049
23,000	0.133	434.8	0.095
23,800	0.264	420.2	0.202
24,700	0.450	404.9	0.371
25,600	0.745	390.6	0.660
26,600	0.960	375.9	0.918
27,200	1.00	367.7	1.00
27,800	0.939	359.7	0.981
28,900	0.587	346.0	0.663
30,150	0.121	331.7	0.149
31,000	0.033	322.6	0.049

[a] 10^{-5} M in 0.1 N_2SO_4. From [10] and [11].
[b] Calculated using $I(\lambda) = I(\bar{\nu})\lambda^{-2}$ followed by normalization of the maximum to unity.

(Table I.9 and Figure I.10). Corrected emission spectra have been reported[10] for phenol and the aromatic amino acids, phenylalanine, tyrosine and tryptophan (Figure I.11).

6. ADDITIONAL CORRECTED EMISSION SPECTRA

Corrected spectra as $I(\bar{\nu})$ versus $\bar{\nu}$ can be found in the compendium by Berlman.[11] Included in that volume are a number of UV-emitting species including indole and phenol, which can be used to obtain corrected emission spectra of proteins. For convenience Berlman's spectra for phenol and indole are provided as Figure I.12. Cresyl violet in methanol has been proposed as a quantum yield and emission spectral standard for red wavelengths.[12] In methanol at 22°C the quantum yield of cresyl violet is reported to be 0.54, with an emission maximum near 614 nm. The use of quinine as a standard has occasionally been questioned.[13–16] Additional discussion about corrected emission spectra can be found in [17–20].

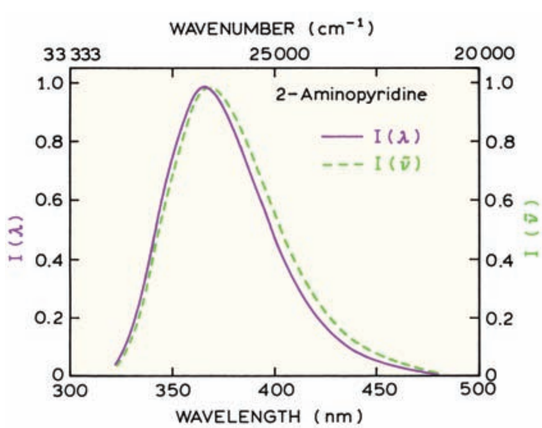

Figure I.10. Corrected emission spectra of 2-aminopyridine in relative quanta per wavenumber interval $I(\bar{\nu})$ and per wavelength interval $I(\lambda)$. See Table I.8 for additional details. From [8] and [9].

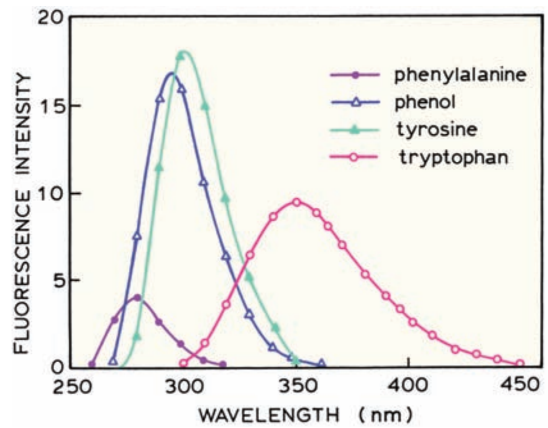

Figure I.11. Corrected emission spectrum ($I(\lambda)$) for phenylalanine (●), phenol (△), tyrosine (▲), and tryptophan (○). The areas underneath the curves are proportional to the quantum yields. Data from [10].

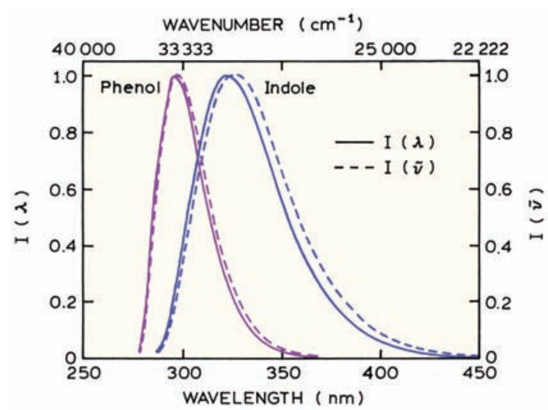

Figure I.12. Corrected emission spectra of phenol in methanol and indole in ethanol. From [11].

REFERENCES

1. Gardecki JA, Maroncelli M. 1998. Set of secondary emission standards for calibration of the spectral responsibility in emission spectroscopy. *Appl Spectrosc* **52**:1179–1189.

2. Pardo A, Reyman D, Poyato JML, Medina F. 1992. Some β-carboline derivatives as fluorescence standards. *J Luminesc* **51**:269–274.
3. Ghiggino KP, Skilton PF, Thistlethwaite PJ. 1985. β-Carboline as a fluorescence standard. *J. Photochem* **31**:113–121.
4. Heller CA, Henry RA, McLaughlin BA, Bliss DE. 1974. Fluorescence spectra and quantum yields: quinine, uranine, 9,10-diphenylanthracene, and 9,10-bis(phenylethynyl) anthracenes. *J Chem Eng Data* **19**(3):214–219.
5. Melhuish WH. 1960. A standard fluorescence spectrum for calibrating spectro-fluorophotometers. *J Phys Chem* **64**:762–764.
6. Lippert EN, Nägele W, Seibold-Blankenstein I, Staiger W, Voss W. 1959. Messung von fluorescenzspektren mit hilfe von spektralphotometern und vergleichsstandards. *Z Anal Chem* **170**:1–18.
7. Schmillen A, Legler R. 1967. *Landolt-Börnstein*, Vol. 3: *Lumineszenz Organischer Substanzen*. Springer-Verlag, New York, pp. 228–229.
8. Testa AC. 1969. Fluorescence quantum yields and standards. *Am Instrum Co, Newsl Luminesc* **4**(4):1–3.
9. Rusakowicz R, Testa AC. 1968. 2-aminopyridine as a standard for low wavelength spectrofluorimetry. *J Phys Chem* **72**:2680–2681.
10. Chen RF. 1967. Fluorescence quantum yields of tryptophan and tyrosine. *Anal Lett* **1**:35–42.
11. Berlman IB. 1971. *Handbook of fluorescence spectra of aromatic molecules*, 2nd ed, Academic Press, New York.
12. Magde D, Brannon JH, Cremers TL, Olmsted J. 1979. Absolute luminescence yield of cresyl violet: a standard for the red. *J Phys Chem* **83**(6):696–699.
13. Chen RF. 1967. Some characteristics of the fluorescence of quinine. *Anal Biochem* **19**:374–387.
14. Fletcher AN. 1968. Fluorescence emission band shift with wavelength of excitation. *J Phys Chem* **72**:2742–2749.
15. Itoh K, Azumi T. 1973. Shift of emission band upon excitation at the long wavelength absorption edge: a preliminary survey for quinine and related compounds. *Chem Phys Lett* **22**(2):395–399.
16. Gill JE. 1969. The fluorescence excitation spectrum of quinine bisulfate. *Photochem Photobiol* **9**:313–322.
17. Melhuish WH. 1972. Absolute spectrofluorometry. *J Res Natl Bur Stand* **76A**:547–560.
18. Credi A, Prodi L. 1996. Correction of luminescence intensity measurements in solution: a simple method to standard spectrofluoroimeters. *EPA Newsl* **58**:50–59.
19. Eaton DF. 1988. Reference materials for fluorescence measurement. *Pure Appl Chem* **60**(7):1107–1114.
20. Zwinkels JC, Gauthier F. 1999. Instrumentation, standards, and procedures used at the National Research Council of Canada for high-accuracy fluorescence measurements. *Anal Chimica Acta* **380**:193–209.

Appendix II

Fluorescence Lifetime Standards

It is valuable to have fluorophores of known lifetimes for use as lifetime standards in time-domain or frequency-domain measurements. Perhaps more important than the actual lifetime is knowledge that the fluorophore displays single-exponential decays. Such fluorophores are useful for testing the time-resolved instruments for systematic errors. We summarized the results from several laboratories on lifetime standards. There is no attempt to compare the values, or to evaluate that values are more reliable. Much of the data is from this laboratory because it was readily available with all the experimental details.

1. NANOSECOND LIFETIME STANDARDS

A series of scintillator fluorophores were characterized as standards for correcting timing errors in photomultiplier tubes.[1] While the decay times were only measured at one or two frequencies, these compounds are thought to display single-exponential decays in ethanol. The decay times are in equilibrium with air, and are not significantly sensitive to temperature (Table II.1). These excitation wavelengths range from 280 to 360 nm, and the emission wavelengths range from 300 to 500 nm (Figure II.1).

One of our most carefully characterized intensity decays is for PPD in ethanol at 20°C, in equilibrium with air.[2] The frequency response was measured with a GHz frequency-domain instrument. No deviations from a single-exponential decay were detected over the entire range of frequencies (Figure II.2).

Table II.1. Nanosecond Reference Fluorophores

Compound[a]	Emission wavelength range	τ (ns)[b]
p-Terphenyl[c]	310–412	1.05
PPD	310–440	1.20
PPO	330–480	1.40
POPOP	370–540	1.35
$(Me)_2$POPOP	390–560	1.45

[a]The abbreviations are: PPD, 2,5-diphenyl-1,3,4-oxadizole; PPO, 2,5-diphenyloxazole; POPOP, *p*-bis[2-(5-phenyloxazolyl)]benzene; dimethyl or $(Me)_2$POPOP, 1,4-bis-2-(4-methyl-5-phenyloxazolyl)-benzene.
[b]These values are judged to be accurate to ±0.2 ns at 10 and 30 MHz. From [1].

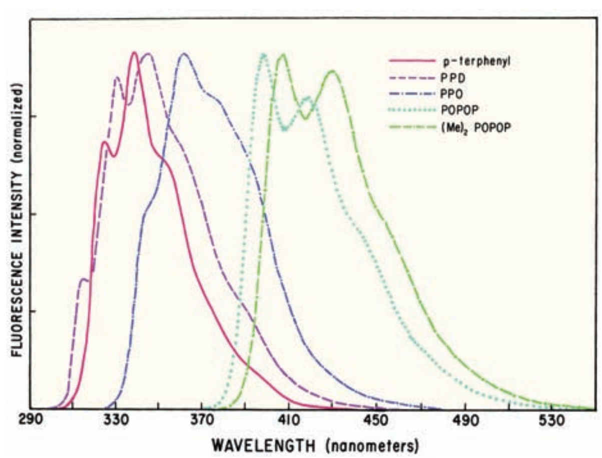

Figure II.1. Emission spectra of nanosecond lifetime reference fluorophores. Reprinted from [1]. Copyright © 1981, with permission from Elsevier Science.

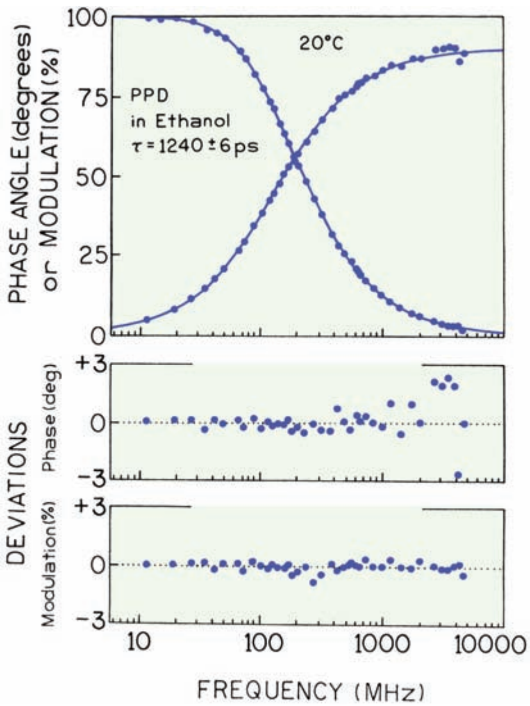

Figure II.2. PPD in ethanol as a single-decay-time standard, in ethanol in equilibrium with air. Reprinted with permission from [2]. Copyright © 1990, American Institute of Physics.

2. PICOSECOND LIFETIME STANDARDS

Derivatives of dimethylamino-stilbene were characterized as lifetime standards with subnanosecond lifetimes[3] (Figure II.3). Excitation wavelengths range up to 420 nm, and emission wavelengths from 340 to over 500 nm (Figure II.4).

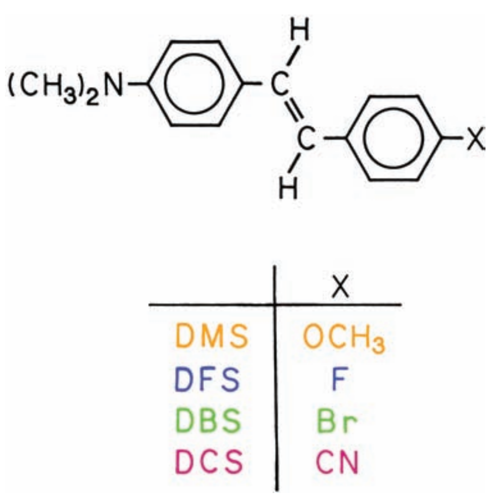

Figure II.3. Picosecond lifetime standard fluorophores. From [3].

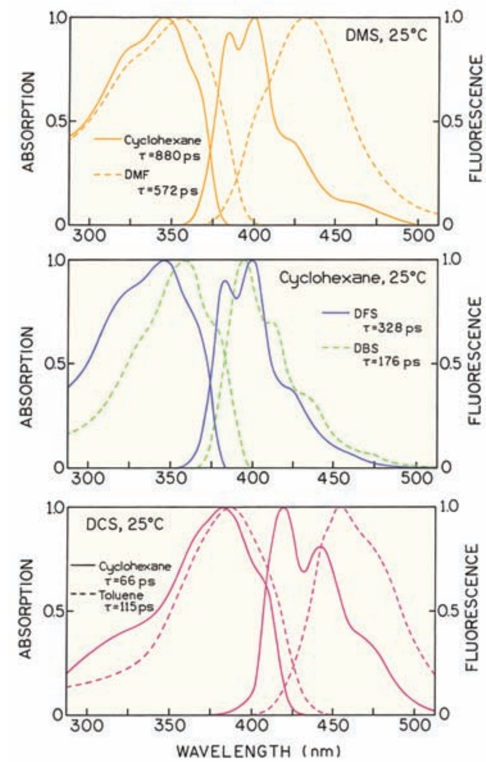

Figure II.4. **Top**: Absorption and fluorescence spectra of DMS in cyclohexane (solid) and N,N'-dimethylformamide (dashed) at 25°C. **Middle**: Absorption and fluorescence spectra of DFS (solid) and DBS (dashed) in cyclohexane at 25°C. **Bottom**: Absorption and fluorescence spectra of DCS in cyclohexane (solid) and toluene (dashed) at 25°C. Revised from [3].

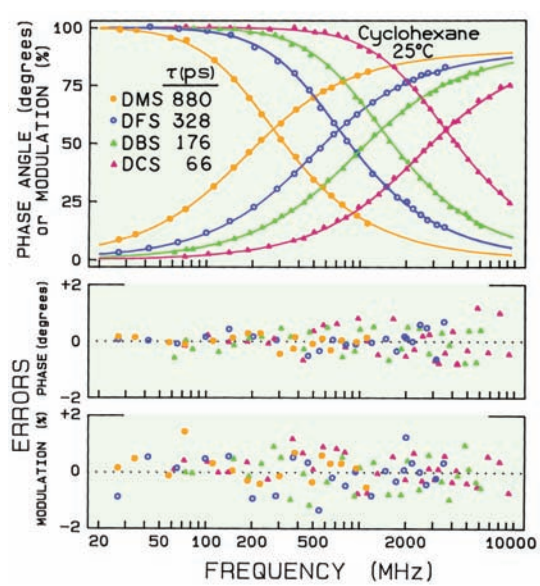

Figure II.5. Representative frequency response of the picosecond lifetime standards. From [3].

Table II.2. Picosecond Lifetime Standards[a]

Compound	No.[a]	Sol-vent[b]	Q[c]	T (°C)	τ (ps)
DMS	1	C	0.59	25	880
	2	C	–	37	771
	3	T	0.32	25	740
	4	T	–	5	921
	5	DMF	0.27	25	572
	6	EA	0.15	25	429
DFS	7	C	–	25	328
	8	C	–	37	252
	9	T	0.16	25	305
	10	T	–	5	433
DBS	11	C	0.11	25	176
	12	C	–	37	133
	13	T	0.12	25	168
	14	T	–	5	248
DCS	15	C	0.06	25	66
	16	C	–	37	57
	17	T	0.06	25	115
	18	T	–	5	186

[a]From [3]. Numbers refer to Figure II.6. These results were obtained from frequency-domain measurements.
[b]C, cyclohexane; T, toluene; DMF, dimethylformamide; EA, ethyl acetate. The excitation wavelength was 365 nm.
[c]Quantum yields.

Representative frequency responses show that the intensity decays are all single exponentials (Figure II.5). The solutions are all in equilibrium with air. The decay times range from 57 to 921 ps (Table II.2 and Figure II.6).

Rose Bengal can serve as a picosecond lifetime standard at longer wavelengths (Figure II.7). Rose Bengal can also be used as a standard for a short rotational correlation time (Figure II.8).

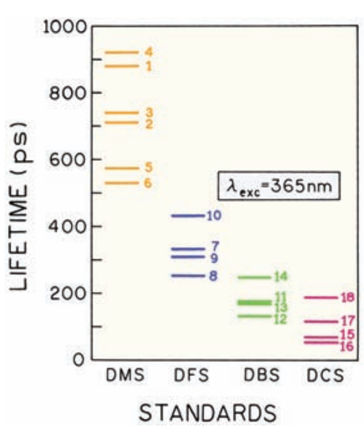

Figure II.6. Lifetimes of the picosecond standards. From [3].

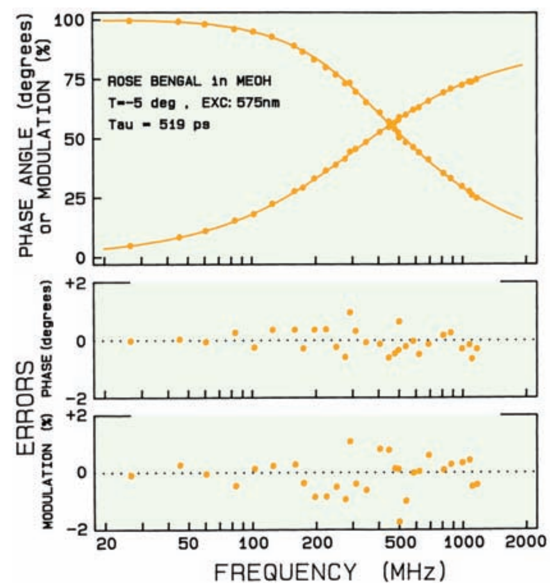

Figure II.7. Rose Bengal as long-wavelength picosecond lifetime standard. For additional lifetime data on Rose Bengal see [4].

3. REPRESENTATIVE FREQUENCY-DOMAIN INTENSITY DECAYS

It can be useful to have access to the actual lifetime data. Representative frequency-domain data for single-exponen-

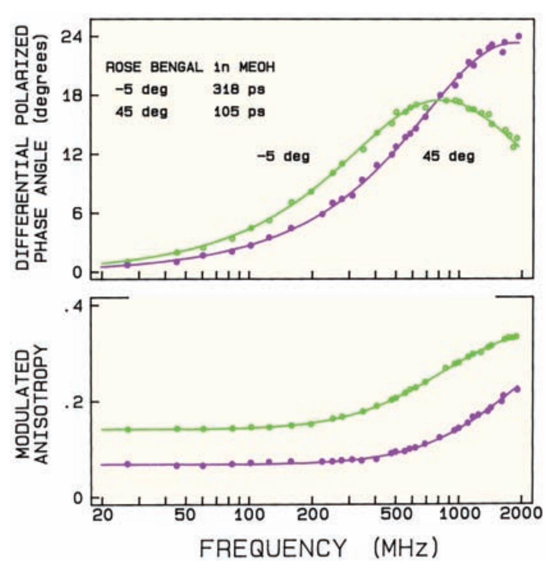

Figure II.8. Rose Bengal as a picosecond correlation time standard. For additional data on Rose Bengal see [4].

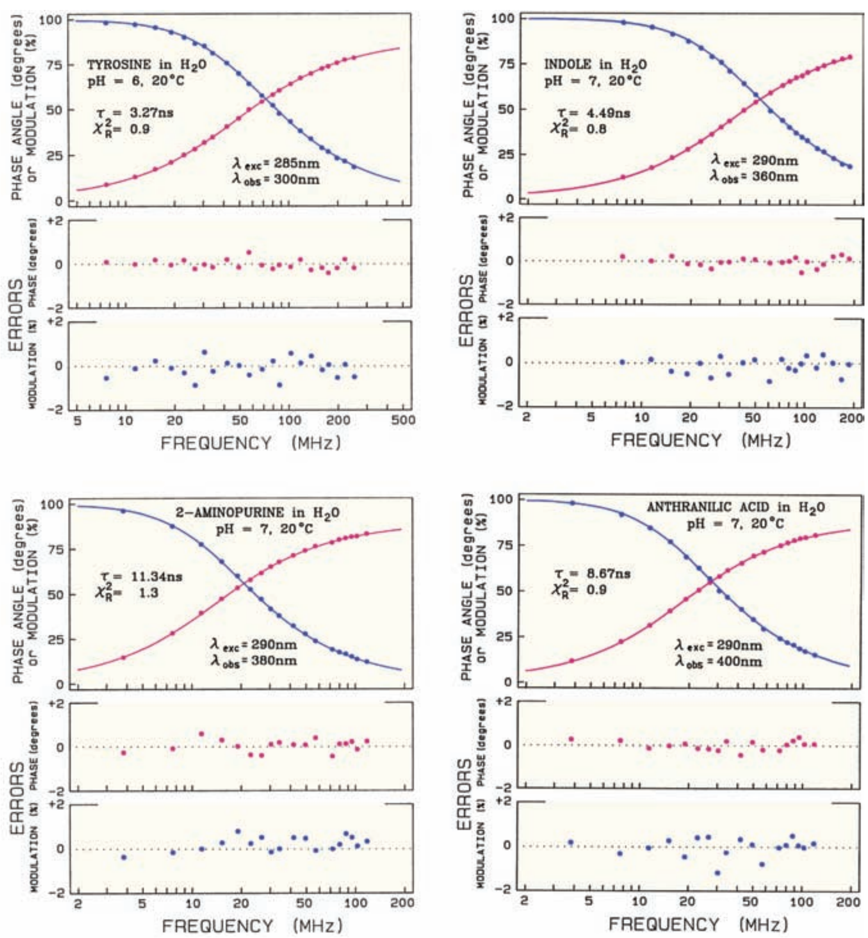

Figure II.9. Representative frequency-domain intensity decays. From [5].

Table II.3. Time-Domain Single Lifetime Standards[a]

Compound	Solvent, 20°C	Emission (nm)	τ (ns)
PPO	cyclohexane (D)	440	1.42
PPO	cyclohexane (U)	440	1.28
Anthracene	cyclohexane (D)	405	5.23
Anthracene	cyclohexane (U)	405	4.10
1-cyanonaphthalene	hexane (D)	345	18.23
1-methylindole	cyclohexane (D)	330	6.24
3-methylindole	cyclohexane (D)	330	4.36
3-methylindole	ethanol (D)	330	8.17
1,2-dimethylindole	ethanol (D)	330	5.71

[a]From [13]. These results were obtained using time-correlated single-photon counting.
[b]D = degassed; U = undegassed.

tial decays as shown in Figure II.9. All samples are in equilibrium with air.[5] Additional frequency-domain data on single-decay-time fluorophores are available in the literature,[6–10] and a cooperative report between several laboratories on lifetime standards is in preparation.[11]

4. TIME-DOMAIN LIFETIME STANDARDS

The need for lifetime standards for time-domain measurements has been recognized for some time.[12] A number of laboratories have suggested samples as single-decay-time standards.[13–17] The data are typically reported only in tables (Tables II.3 to II.5), so representative figures are not available. The use of collisional quenching to obtain different lifetimes[17–18] is no longer recommended for lifetime standards due to the possibility of transient effects and nonexponential decays. Quinine is not recommended as a lifetime standard due to the presence of a multi-exponential decay.[19-20]

Table II.4. Single-Exponential Lifetime Standards

Sample[a]	λ_{em} (nm)	τ (ns[a])
Anthracene	380	5.47
PPO	400	1.60
POPOP	400	1.38
9-cyanoathracene	440	14.76

[a]All samples in ethanol. The lifetimes were measured by time-correlated single-photon counting. From [14]. The paper is unclear on purging, but the values seem consistent with digassed samples.

Table II.5. Single-Exponential Standards[a]

Fluorophore	τ (ns)
POPOP in cyclohexane	1.14 ± 0.01
POPOP in EtOH	1.32 ± 0.01
POPOP in aq EtOH	0.87 ± 0.01
Anthracene in EtOH	4.21 ± 0.02
9-Cyanoanthracene in EtOH	11.85 ± 0.03

[a]All measurements were at 25°C, in equilibrium with air, by time-correlated single photon counting. From [17].

Appendix III

Additional Reading

It is not possible in a single volume to completely describe the molecular photophysics and the application of fluorescence spectroscopy. The following books are recommended for additional details on specialized topics. This listing is not intended to be inclusive, and the author apologizes for absence of important citations.

1. TIME-RESOLVED MEASUREMENTS

Chemical applications of ultrafast spectroscopy 1986. Fleming, GR. Oxford University Press, New York.

Excited state lifetime measurements 1983. Demas JN. Academic Press, New York, pp. 267.

Time-correlated single photon counting 1984. O'Connor DV, Phillips D. Academic Press, New York.

Topics in fluorescence spectroscopy. Vol 1. 1991. Lakowicz JR, ed. Plenum Press, New York.

2. SPECTRA PROPERTIES OF FLUOROPHORES

Energy transfer parameters of aromatic compounds. 1973. Berlman IB. Academic Press, New York.

Biological techniques: fluorescent and luminescent probes for biological activity. 1999. Mason WT. Academic Press, New York.

Handbook of fluorescence spectra of aromatic molecules, 2nd ed. 1971. Berlman IB. Academic Press, New York.

Handbook of fluorescent probes and research chemicals, 9th ed. 2003. Haugland RP, ed. Molecular Probes Inc.

Landolt-Börnstein: zahlenwerte und funktionen aus naturwissenschaften und technik. 1967. Serie N. Springer-Verlag, Berlin.

Molecular luminescence spectroscopy: methods and applications: part 1. 1985. Schulman SG, ed. John Wiley & Sons, New York.

Molecular luminescence spectroscopy: methods and applications: part 2. 1988. Schulman SG, ed. John Wiley & Sons, New York.

Molecular luminescence spectroscopy: methods and applications: part 3. 1993. Schulman SG, ed. John Wiley & Sons, New York.

Organic luminescent materials. 1984. Krasovitskii BM, Bolotin BM (Vopian VG, transl). VCH Publishers, Germany.

Practical fluorescence, 2nd ed. 1990. Guilbault GG, ed. Marcel Dekker, New York.

3. THEORY OF FLUORESCENCE AND PHOTOPHYSICS

Photophysics of aromatic molecules. 1970. Birks JB. Wiley Interscience, New York.

Organic molecular photophysics, Vol 1. 1973. Birks JB, ed. John Wiley & Sons, New York.

Organic molecular photophysics, Vol 2. 1975. Birks JB, ed. John Wiley & Sons, New York.

Fotoluminescencja roztworow. 1992. Kawski A. Wydawnictwo Naukowe PWN, Warszawa.

The 1970 and 1973 books by Birks are classic works that summarize organic molecular photophysics. These books start by describing fluorescence from a quantum mechanical perspective, and contain valuable detailed tables and figures that summarize spectral properties and photophysical parameters. Unfortunately, these books are no longer in print, but they may be found in some libraries.

4. REVIEWS OF FLUORESCENCE SPECTROSCOPY

Methods in enzymology, Vol. 278: *Fluorescence spectroscopy*. 1997. Brand L, Johnson ML. Academic Press, New York.

Molecular fluorescence, phosphorescence, and chemiluminescence spectrometry. 2004. Powe AM, Fletcher KA, St. Luce NN, Lowry M, Neal S, McCarroll ME, Oldham PB, McGown LB, Warner IM. *Anal Chem* **76**:4614–4634. This review is published about every two years.

Resonance energy transfer: theory and data. 1991. Wieb Van Der Meer B, Coker G, Chen S-Y. Wiley-VCH, New York.

Topics in fluorescence spectroscopy, Vol 2: *Principles*. 1991. Lakowicz JR, ed. Plenum Press, New York. Provides information on the biochemical applications of anisotropy, quenching, energy transfer, least-square analysis, and oriented systems.

Topics in fluorescence spectroscopy, Vol 3: *Biochemical applications*. 1992. Lakowicz JR, ed. Plenum Press, New York. Describes the spectral properties of intrinsic biological fluorophores and labeled macromolecules. There are chapters on proteins, membranes and nucleic acids.

Topics in fluorescence spectroscopy, Vol 7: *DNA technology 2003*. Lakowicz JR, ed. Kluwer Academic/Plenum Publishers, New York.

5. BIOCHEMICAL FLUORESCENCE

Analytical use of fluorescent probes in oncology. 1996. Kohen E, Hirschberg JG, eds. Plenum Press, New York.

Applications of fluorescence in the biomedical sciences. 1986. Taylor DL, Waggoner AS, Murphy RF, Lanni F, Birge RR, eds. Alan R. Liss, New York.

Biophysical and biochemical aspects of fluorescence spectroscopy. 1991. Dewey TG, ed. Plenum Press, New York.

Biotechnology applications of microinjection, microscopic imaging, and fluorescence. 1993. Bach PH, Reynolds CH, Clark JM, Mottley J, Poole PL, eds. Plenum Press, New York.

Fluorescent and luminescent probes for biological activity: a practical guide to technology for quantitative real-time analysis, 2nd ed. 1999. Mason WT, ed. Academic Press, San Diego.

Fluorometric analysis in biomedical chemistry. 1987. Ichinose N, Schwedt G, Schnepel FM, Adachi K. John Wiley & Sons.

Fluorescence spectroscopy. 1997. Brand L, Johnson ML, eds. Academic Press, New York.

Methods in cell biology, Vol 58: *Green fluorescent proteins*. 1999. Sullivan KF, Kay SA, eds. Academic Press, San Diego.

Spectroscopic membrane probes, Vol 1. 1988. Loew LM, ed. CRC Press, Boca Raton, FL.

Spectroscopic membrane probes, Vol 2. 1988. Loew LM, ed. CRC Press, Boca Raton, FL.

Spectroscopic membrane probes, Vol 3. 1988. Loew LM, ed. CRC Press, Boca Raton, FL.

6. PROTEIN FLUORESCENCE

Fluorescence and phosphorescence of proteins and nucleic acids. 1967. Konev SV. (Udenfriend S, transl). Plenum Press, New York.

Luminescence of polypeptides and proteins. 1971. Longworth JW. In *Excited states of proteins and nucleic acids*, pp. 319–484. Steiner RF, Weinryb I, eds. Plenum Press, New York.

Luminescent spectroscopy of proteins. 1993. Permyakov EA. CRC Press, Boca Raton, FL.

Ultraviolet spectroscopy of proteins. 1981. Demchenko AP. Springer-Verlag, New York.

7. DATA ANALYSIS AND NONLINEAR LEAST SQUARES

Data reduction and error analysis for the physical sciences, 2nd ed. 1992. Bevington PR, Robinson DK. McGraw-Hill, Boston.

Evaluation and propagation of confidence intervals in nonlinear, asymmetrical variance spaces: analysis of ligand binding data. 1983. Johnson ML. *Biophy J* **44**:101–106.

An introduction to error analysis. 1982. Taylor JR. University Science Books, California.

Methods in enzymology, Vol 240: *Numerical computer methods*. 1994. Johnson ML, Brand L, eds. Academic Press, New York.

Methods in enzymology, Vol 210: *Numerical computer methods*. 1992. Brand L, Johnson ML, eds. Academic Press, New York.

Statistics in spectroscopy. 1991. Mark H, Workman J. Academic Press, New York.

8. PHOTOCHEMISTRY

Essentials of molecular photochemistry. 1991. Gilbert A, Baggott J. CRC Press, Boca Raton, FL.

Fundamentals of photoinduced electron transfer. 1993. Kavarnos GJ. VCH Publishers, New York.

Modern molecular photochemistry. 1978. Turro NJ. Benjamin/Cummings Publishing, San Francisco.

Photochemistry and photophysics, Vol 1. 1990. Rabek JF. CRC Press, Boca Raton, FL.

Photochemistry and photophysics, Vol 2. 1990. Rabek JF. CRC Press, Boca Raton, FL.

Photochemistry and photophysics, Vol 3. 1991. Rabek JF. CRC Press, Boca Raton, FL.

Principles and applications of photochemistry. 1988. Wayne RP. Oxford University Press, New York.

For most applications of fluorescence, photochemical effects are to be avoided. However, it can be valuable to understand that chemical reactions occur in the excited state.

9. FLOW CYTOMETRY

Flow cytometry. 1992. Givan AL. Wiley-Liss, New York.

Practical flow cytometry. 2nd ed. 1988. Shapiro HM. Alan R. Liss, New York.

10. PHOSPHORESCENCE

Phosphorimetry: theory, instrumentation, and applications. 1990. Hurtubise RJ. VCH Publishers, New York.

11. FLUORESCENCE SENSING

Chemical sensors and biosensors for medical and biological applications. 1998. Spichiger-Keller UE. Wiley-VCH, Weinheim.

Sensors and actuators B. 1996. Part 1: Plenary and Parallel Sessions; Part 2: Poster Sessions. Kunz RE, ed. Proceedings of the Third European Conference on Optical Chemical Sensors and Biosensors. Europt(R)ode III. Elsevier Publishers, New York.

Topics in fluorescence spectroscopy, Vol 4: *Probe design and chemical sensing*. 1994. Lakowicz JR, ed. Plenum Press, New York.

Biosensors in the body—continuous in vivo monitoring. 1997. Fraser DM, ed. Biomaterials Science and Engineering Series, Wiley, New York.

12. IMMUNOASSAYS

Applications of fluorescence in immunoassays. 1991. Hemmila IA. John Wiley & Sons, New York.

Luminescence immunoassay and molecular applications. 1990. Van Dyke K, Van Dyke R. CRC Press, Boca Raton, FL.

13. APPLICATIONS OF FLUORESCENCE

Analytical use of fluorescent probes in oncology. 1996. Kohen E, Hirschberg JG, eds. Plenum Press, New York.

Fluorescent chemosensors for ion and molecule recognition. 1992. Czarnik AW, ed. *ACS Symposium Series*, Vol 538.

Fluorescent probes in cellular and molecular biology. 1994. Slavik J. CRC Press, Boca Raton, FL.

Fluorescence microscopy and fluorescent probes. 1996. Slavik J, ed. Plenum Press, New York.

Fluorescence spectroscopy. 1993. Wolfbeis OS, ed. Springer-Verlag, New York.

Sensors and actuators B: chemical. 1994. Baldini F, ed. Elsevier Press. Vol B2.(1–3).

Applied fluorescence in chemistry, biology and medicine. 1999. Rettig W, Strehmel B, Schrader S, Seifert H. Springer, New York.

New trends in fluorescence spectroscopy. 2001. Valeur B, Brochon J-C, eds. Springer, New York.

Fluorescence spectroscopy, imaging, and probes. 2002. Kraayenhof R, Visser AJWG, Gerritsen HC, eds. Springer, New York.

14. MULTIPHOTON EXCITATION

Topics in fluorescence spectroscopy, Vol 5: *Non-linear and two-photon induced fluorescence*. 1997. Lakowicz JR, ed. Plenum Press, New York.

Fluorescence microscopy and fluorescent probes, Vol 2. 1998. Slavik J, ed. Plenum Press, New York.

15. INFRARED AND NIR FLUORESCENCE

Infrared absorbing dyes. 1990. Matsuoka M. Plenum Press, New York.

Phthalocyanines: properties and applications. 1989. Leznoff CC, Lever ABP, eds. VCH Publishers, New York.

Near-infrared dyes for high technology applications. 1998. Daehne S, Resch-Genger U, and Wolfbeis OS, eds. Kluwer Academic Publishers, Boston.

16. LASERS

Fundamentals of laser optics. 1994. Iga K. (Miles RB, tech ed). Plenum Press, New York.

Principles of lasers, 4th ed. 1998. Svelto O. (Hanna DC, ed, transl) Plenum Press, New York.

An introduction to laser spectroscopy. 2002. Andrews DL, Deminov AA, eds. Kluwer Academic/Plenum Publishers, New York.

Laser spectroscopy: basic concepts and instrumentation, 3rd ed. 2003. Demtroder W. Springer, New York.

17. FLUORESCENCE MICROSCOPY

Chemical analysis: a series of monographs on analytical chemistry and its applications. 1996. Fluorescence Imaging Spectroscopy and Microscopy, Vol 137. Wang XF, and Herman B, eds. John Wiley & Sons, New York.

Fluorescence imaging spectroscopy and microscopy. 1996. Wang XF, Herman B. John Wiley & Sons, New York.

Handbook of confocal microscopy, 2nd ed. 1995. Pawley JB, ed. Plenum Press, New York. See also the First Edition, 1990.

Methods in cell biology, Vol 38: *Cell biological applications of confocal microscopy*. 1993. Matsumoto B, ed. Academic Press, New York.

Methods in cell biology, Vol 40: *A practical guide to the study of calcium in living cells*. 1994. Nuccitelli R, ed. Academic Press, New York.

Optical microscopy, emerging methods and applications. 1993. Herman B, Lemasters JJ. Academic Press, New York.

Optical microscopy for biology. 1990. Herman B, Jacobson K, eds. Wiley-Liss, New York.

Fluorescent microscopy and fluorescent probes, Vol 2. 1998. Slavik J, ed. Plenum, New York.

18. METAL–LIGAND COMPLEXES AND UNUSUAL LUMOPHORES

Molecular level artificial photosynthetic materials. 1997. Meyer GJ, ed. John Wiley & Sons, New York.

Photochemistry of polypyridine and porphyrin complexes. 1992. Kalyanasundaram K. Academic Press, New York.

Ru(II) polypyridine complexes: photophysics, photochemistry, electrochemistry, and chemiluminescence. 1988. Juris A, Balzani V, Barigelletti F, Campagna S, Belser P, Von Zelewsky A. *Coord Chem Rev* **84**:85–277.

19. SINGLE-MOLECULE DETECTION

Selective spectroscopy of single molecules. 2003. Osad'ko IS. Springer, New York.

Single molecule detection in solution methods and applications. 2002. Zander Ch, Enderlein J, Keller RA, eds. Wiley-Vch, Darmstadt, Germany.

Single molecule spectroscopy: Nobel conference letters. 2001. Rigler R, Orrit M, and Basche T. Springer, New York.

20. FLUORESCENCE CORRELATION SPECTROSCOPY

Fluorescence correlation spectroscopy theory and applications. 2001. Rigler R, Elson ES. Springer, New York.

21. BIOPHOTONICS

Methods in enzymology, Vol. 360: *Biophotonics, part a 2003*. Marriott G, Parker I, eds. Academic Press, New York.

Methods in Enzymology, Vol. 361: *Biophotonics part b 2003*. Marriott G, Parker I, eds. Academic Press, New York.

Introduction to biophotonics. 2003. Prasad PN, Wiley-Interscience, New York.

22. NANOPARTICLES

Nanoparticles. 2004. Rotello V, ed. Kluwer Academic/Plenum Publishers, New York.

Optical properties of semiconductor nanocrystals. 1998. Gaponenko SV. Cambridge University Press, New York.

23. METALLIC PARTICLES

Electronic excitations at metal surfaces. 1997. Liebsch A. Plenum Press, New York.

Metal nanoparticles synthesis, characterization, and applications. 2002. Feldheim DL, Foss CA, eds. Marcel Dekker, New York.

24. BOOKS ON FLUORESCENCE

Introduction to fluorescence spectroscopy. 1999. Sharma A, Schulman SG, eds. Wiley-Interscience, New York.

Molecular fluorescence principles and applications. 2002. Valeur B. Wiley-VCH, New York.

Who's who in fluorescence 2004. 2004. Geddes CD, Lakowicz JR, eds. Kluwer Academic/Plenum Publishers, New York.

Answers to Problems

CHAPTER 1

A1.1. A. The natural lifetimes and radiative decay rates can be calculated from the quantum yields and experimental lifetimes:

$$\tau_N(\text{eosin}) = \tau/Q = \frac{3.1}{0.65} = 4.77 \text{ ns} \qquad (1.18)$$

$$\tau_N(\text{EB}) = \tau Q = \frac{0.61}{0.12} = 5.08 \text{ ns} \qquad (1.19)$$

Hence eosin and erythrosin B have similar natural lifetimes and radiative decay rates (eq. 1.3). This is because both molecules have similar absorption and emission wavelengths and extinction coefficients (eq. 1.4).

The non-radiative decay rates can be calculated from eq. 1.2, which can be rearranged to

$$\frac{1}{\tau} - \frac{1}{\tau_N} = k_{nr} \qquad (1.20)$$

For eosin and erythrosin B the non-radiative decay rates are 1.1 x 10^8 s^{-1} and 1.44 x 10^9 s^{-1}, respectively. The larger non-radiative decay rate of erythrosin B is the reason for its shorter lifetime and lower quantum yield than eosin.

B. The phosphorescence quantum yield (Q_p) can be estimated from an expression analogous to eq 1.1:

$$Q_p = \frac{\Gamma_p}{\Gamma_p + k_{nr}} \qquad (1.21)$$

Using the assumed natural lifetime of 10 ms, and k_{nr} = 1 x 10^8 s^{-1}, $Q_p = 10^{-6}$. If k_{nr} is larger, Q_p is still smaller, so that Q_p ; 10^{-7} for ErB. This explains why it is difficult to observe phosphorescence at room temperature: most of the molecules that undergo intersystem crossing return to the ground state by non-radiative paths prior to emission.

A1.2. The quantum yield (Q_2) of S_2 can be estimated from

$$Q_2 = \frac{\Gamma}{\Gamma + k_{nr}} \qquad (1.22)$$

The value of k_{nr} is given by the rate of internal conversion to S_1, 10^{13} s^{-1}. Using Γ = 2.1 x 10^8, one can estimate Q_2 = 2 x 10^{-5}. Observation of emission from S_2 is unlikely because the molecules relax to S_1 prior to emission from S_2.

A1.3. The energy spacing between the various vibrational energy levels is revealed by the emission spectrum of perylene (Figure 1.3). The individual emission maxima (and hence vibrational energy levels) are about 1500 cm^{-1} apart. The Boltzmann distribution describes the relative number of perylene molecules in the 0 and 1 vibrational states. The ratio (R) of molecules in each state is given by

$$R = e^{-\Delta E/kT} \qquad (1.23)$$

where ΔE is the energy difference, k is the Boltzmann constant, and T is the temperature in degrees kelvin (K). Assuming a room temperature of 300 K, this ratio is about 0.01. Hence most molecules will be present in the lowest vibrational state, and light absorption results mainly from molecules in this energy level. Because of the larger energy difference between S_0 and S_1, essentially no fluorophores can populate S_1 as a result of thermal energy.

A1.4. A. The anisotropy of the DENS-labeled protein is given by eq. 1.10. Using $\tau = \theta$, the steady-state anisotropy is expected to be 0.15.

B. If the protein binds to the larger antibody, its rotational correlation time will increase to 100 ns or longer. Hence the anisotropy will be 0.23 or higher. Such increases in anisotropy upon antigen–antibody binding are the basis of the fluorescence polarization immunoassays, which are used to detect drugs, peptides, and small proteins in clinical samples.

A1.5. The dependence of transfer efficiency on distance (r) between a donor and acceptor can be calculated using eq. 1.12 (Figure 1.41). At $r = R_0$ the efficiency is 50%; at $r = 0.5R_0$, $E = 0.98$; and at $r = 2R_0$, $E = 0.02$.

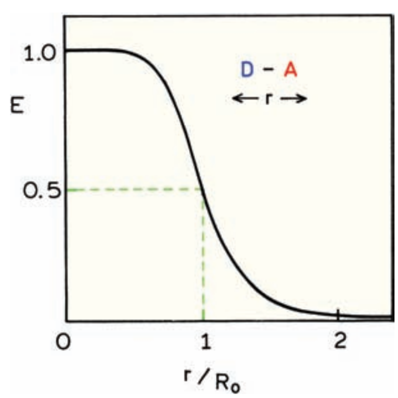

Figure 1.41. Effect of donor-to-acceptor distance on transfer efficiency.

A1.6. The distance can be calculated for the relative quantum yield of the donor in the presence or absence of the acceptor. The data in Figure 1.37 reveal a relative tryptophan intensity of 0.37, assuming the anthraniloyl group does not contribute at 340 nm. A transfer efficiency of 63% corresponds (see eq. 1.12) to a distance of $r = 0.92R_0$ = 27.7 Å.

In reality the actual calculation is more complex, and the tryptophan intensity needs to be corrected for anthraniloyl emission.[42] When this is done the transfer efficiency is found to be about 63%, and the distance near 31.9 Å.

A1.7. The changes in λ_{max}, K, and r shown in Figure 1.38 are the result of the tryptophan residue being exposed to or shielded from the water. Increases in λ_{max} and K indicate increased exposure to water, and decreases in λ_{max} and K indicate decreases in exposure to water. Increases and decreases in r indicate a less mobile and more mobile tryptophan residue, respectively. The three parameter values show a cyclical behavior with a period of about 3.5 amino acid residues per cycle. This suggests that the MLCK peptide is in an α-helical state when bound to calmodulin (Figure 1.42). The spectral changes seen in Figure 1.38 are the result of the tryptophan residue being alternately exposed to water or shielded between the MLCK peptide and calmodulin as its position is shifted along the peptide chain.

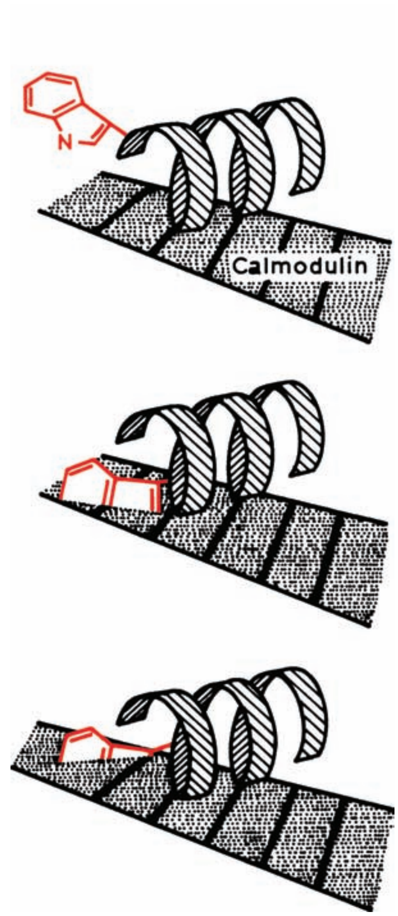

Figure 1.42. Schematic of the interactions of the O-helical MLCK peptide with calmodulin. The position of the single tryptophan residue is moved along the helix in 16 synthetic peptides. Reprinted with permission from [40]. (O'Neil KT, Wolfe HR, Erickson-Vitanen S, DeGrado WF. 1987. Fluorescence properties of calmodulin-binding peptides reflect O-helical periodicity. *Science* **236**:1454–1456, Copyright © 1987, American Association for the Advancement of Science.)

A1.8. Figure 1.40 shows that the donor intensity increases and the acceptor intensity decreases upon addition of cAMP and PKI. These spectral changes indicate a decrease in RET. The donor and acceptor must move further apart when the protein binds cAMP or PKI. According to publications[43] the C and R subunits remain associated in the presence of cAMP, but change this relative conformation (Figure 1.43). PKI was said to dissociate the subunit.

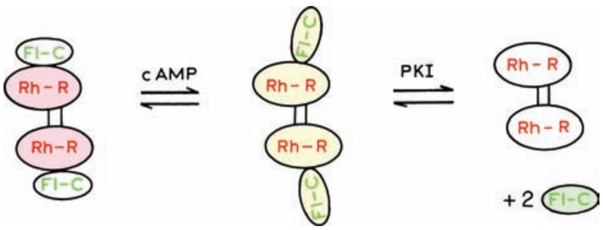

Figure 1.43. Effect of cAMP and protein kinase inhibitor (PKI) on the structure and association of cAMP-dependent protein kinase. The holoenzyme consists of two catalytic and two regulatory subunits.

CHAPTER 2

A2.1. The true optical density is 10. Because of stray light the lowest percent transmission (%T) you can measure is 0.01%. The %T of the rhodamine solution is much less than 0.01%. In fact $I/I_0 = 10^{-10}$ and %$T = 10^{-8}$%. Hence your instrument will report an optical density of 4.0. The calculated concentration of rhodamine B would be 4 x 10^{-5} M, 2.5-fold less than the true concentration.

A2.2. The concentrations of solutions are 10^{-5} and 10^{-7} M, respectively. A 1% error in %T means the OD can be

$$\mathrm{OD} = \log \frac{I_0}{I} = \log \frac{1}{0.51} \quad \text{or} \quad \log \frac{1}{0.49} \tag{2.13}$$

Hence the concentration can be from 0.97 x 10^{-5} to 1.03 x 10^{-5} M.

For the more dilute solution, the 1% error results in a large error in the concentration:

$$\mathrm{OD} = \log \frac{I_0}{I} = \log \frac{1.00}{1.00} \quad \text{or} \quad \log \frac{1.0}{0.98} \tag{2.14}$$

The measured OD ranges from 0 to 0.009, so the calculated concentration ranges from 0 to 2.9 x 10^{-7} M. This shows that it is difficult to determine the concentration from low optical densities. In contrast, it is easy to obtain emission spectra with optical densities near 0.003.

CHAPTER 3

A3.1. Binding of the protein to membranes or nucleic acids could be detected by several types of measurements. The most obvious experiment would be to look for changes in the intrinsic tryptophan fluorescence upon mixing with lipid bilayers or nucleic acids. In the case of membranes one might expect the tryptophan emission to shift to shorter wavelengths due to shielding of the indole moiety from water. The blue shift of the emission is also likely to be accompanied by an increase in the tryptophan emission intensity. In the case of nucleic acids, tryptophan residues are typically quenched when bound to DNA, so that a decrease in the emission intensity is expected.

Anisotropy measurements of the tryptophan emission could also be used to detect binding. In this case it is difficult to predict the direction of the changes. In general one expects binding to result in a longer correlation time and higher anisotropy (see eq. 1.10), and an increase of the tryptophan anisotropy is likely upon binding to proteins. However, the anisotropy increase may be smaller than expected if the tryptophan lifetime increases on binding to the membranes (eq. 1.10).

In the case of protein binding to nucleic acids, it is difficult to predict the anisotropy change. The tryptophan residues would now be in two states, free (F) and bound (B), and the anisotropy given by

$$r = r_F f_F + r_B f_B, \tag{3.2}$$

where f_F and f_B represent the fraction of the total fluorescence from the protein in each state. If the protein is completely quenched on binding to DNA, then the anisotropy will not change because $f_B = 0$. If the protein is partially quenched the anisotropy will probably increase, but less than expected due to the small contribution of the DNA-bound protein by the total fluorescence.

Energy transfer can also be used to detect protein binding. Neither DNA nor model membranes possess chromophores that can serve as acceptors for the tryptophan fluorescence. Hence it is necessary to add extrinsic probes. Suitable acceptors would be probes that absorb near 350 nm, the emission maximum of most proteins. Numerous membranes and nucleic-acid probes absorb near 350 nm. The membranes could be labeled with DPH (Figure 1.18), which absorbs near 350 nm. If the protein is bound to DPH-labeled membranes, its emission would be quenched by resonance energy transfer to DPH. Similarly, DNA could be labeled with DAPI (Figure 3.23). An advantage of using RET is that through-space quenching occurs irrespective of the details of the binding interactions. Even if there were no change in the intrinsic tryptophan emission upon binding to lipids or nucleic acids, one still expects quenching of the tryptophan when bound to acceptor-labeled membranes or nucleic acids.

A3.2. A. The data in Figure 3.48 can be used to determine the value of F_0/F at each [Cl$^-$], where $F_0 = 1.0$ is the SPQ fluorescence intensity in the absence of Cl$^-$, and F is the intensity at each Cl$^-$ concentration. These values are plotted in Figure 3.49. Using Stern-Volmer eq. 1.6, one obtains $K = 124$ M^{-1}, which is in good agreement with the literature value[182] of 118 M^{-1}.

B. The value of F_0/F and τ_0/τ for 0.103 M Cl$^-$ can be found from eq. 1.6. Using $K = 118$ M^{-1}, one obtains $F_0/F = \tau_0/\tau = 13.15$. Hence the intensity of SPQ is $F = 0.076$, relative to the intensity in the absence of Cl$^-$, $F_0 = 1.0$. The lifetime is expected to be $\tau = 26.3/13.15 = 2.0$ ns.

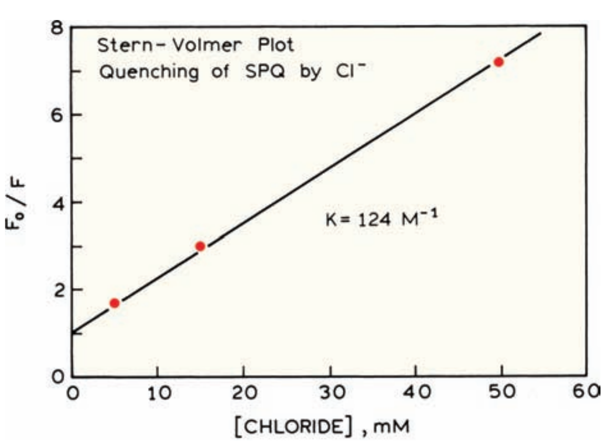

Figure 3.49. Stern-Volmer plot for the quenching of SPQ by chloride.

C. At [Cl$^-$] = 0.075 M, $F = 0.102$ and $\tau = 2.67$.

D. The Stern-Volmer quenching constant of SPQ was determined in the absence of macromolecules. It is possible that SPQ binds to proteins or membranes in blood serum. This could change the Stern-Volmer quenching constant by protecting SPQ from collisional quenching. Also, binding to macromolecules could alter τ_0, the unquenched lifetime. Hence it is necessary to determine whether the quenching constant of SPQ is the same in blood serum as in protein-free solutions.

A3.3. A. The dissociation reaction of the probe (P_B) and analyte (A) is given by

$$P_B = A + P_B, \tag{3.3}$$

where B and F refer to the free and bound forms of the probe. The fraction of free and bound probe is related to the dissociation constant by

$$K_D = \frac{[P_F]}{[P_B]}[A] \tag{3.4}$$

For the non-ratiometric probe Calcium Green, the fluorescein intensity is given by

$$F = q_F C_F + q_B C_B, \tag{3.5}$$

where q_i are the relative quantum yields, C_i the molecular fraction in each form, and $C_F + C_B = 1.0$. The fluorescent intensities when all the probe is free is $F_{min} = kq_F C$, and then all the probe is bound in $F_{max} = kq_B C$, where k is an instrumental constant.

Equation 3.5 can be used to derive expressions for C_B and C_F in terms of the relative intensities:

$$F_B = \frac{F - F_{min}}{F_{max} - F_{min}} \tag{3.6}$$

$$F_F = \frac{F_{max} - F}{F_{max} - F_{min}} \tag{3.7}$$

The fractions C_B and C_F can be substituted for the probe concentration in (3.4), yielding

$$[A] = [\mathrm{Ca}^{2+}] = K_\mathrm{D}\frac{F - F_\mathrm{max}}{F_\mathrm{max} - F} \tag{3.8}$$

B. The fluorescence intensity (F_1 or F_2) observed with each excitation wavelength (1 or 2) depends on the intensity and the concentrations (C_F and C_B) of the free (S_{f1} or S_{f2}), or bound (S_{b1} or S_{b2}), forms at each excitation wavelength:

$$F_1 = S_{f1}C_\mathrm{F} + S_{b1}C_\mathrm{B}, \tag{3.9}$$
$$F_2 = S_{f2}C_\mathrm{F} + S_{b2}C_\mathrm{B}. \tag{3.10}$$

The term S_i depends on the absorption coefficient and relative quantum yield of Fura-2 at each wavelength.

Let $R = F_1/F_2$ be the ratio of intensities. In the absence and presence of saturating Ca^{2+},

$$R_\mathrm{min} = S_{f1}/S_{f2}, \tag{3.11}$$
$$R_\mathrm{max} = S_{b1}/S_{b2}. \tag{3.12}$$

Using the definition of the dissociate constant,

$$[\mathrm{Ca}^{2+}] = \frac{C_\mathrm{B}}{C_\mathrm{F}}K_\mathrm{D} \tag{3.13}$$

one obtains

$$[\mathrm{Ca}^{2+}] = K_\mathrm{D}\frac{R - R_\mathrm{max}}{R_\mathrm{min} - R}\left(\frac{S_{f2}}{f_{b2}}\right) \tag{3.14}$$

Hence one can measure the $[\mathrm{Ca}^{2+}]$ from these ratios of the emission intensities at two excitation wavelengths. However, one needs control measurements, which are the ratio of the intensities of the free and bound forms measured at one excitation wavelength, as well as measurements of R_min and R_max.[183]

CHAPTER 4

A4.1. Calculation of the lifetimes from intensity decay is straightforward. The initial intensity decreases to 0.37 (=1/3) of the initial value at t = 5 ns. Hence, the lifetime is 5 ns.

From Figure 4.2 the phase angle is seen to be about 60 degrees. Using $\omega = 2\pi \cdot 80$ MHz and $\tau_\phi = \omega^{-1}$ [tan ϕ] one finds τ = 3.4 ns. The modulation of the emission relative to the excitation is near 0.37. Using eq. 4.6 one finds τ_m = 5.0 ns. Since the phase and modulation lifetimes are not equal, and since $\tau_\mathrm{m} > \tau_\phi$, the intensity decay is heterogeneous. Of course, it is difficult to read precise values from Figure 4.2.

A4.2. The fractional intensity of the 0.62-ns component can be calculated using eq. 4.28, and is found to be 0.042 or 4%.

A4.3. The short lifetime was assigned to the stacked conformation of FAD. For the open form the lifetime of the flavin is reduced from τ_0 = 4.89 ns to τ = 3.38 ns due to collisions with the adenine. The collision frequency is given by $k = \tau^{-1} - \tau_0^{-1} = 9 \times 10^7$/s.

A4.4. In the presence of quencher the intensity decay is given by

$$I(t) = 0.5 \exp(-t/0.5) + 0.5 \exp(-t/5) \tag{4.42}$$

The α_1 and α_2 values remain the same. The fact that the first tryptophan is quenched tenfold is accounted for by the $\alpha_i\tau_i$ products, $\alpha_1\tau_1$ = 0.25 and $\alpha_2\tau_2$ = 2.5. Using eq. 4.29 one can calculate $\bar{\tau}$ = 4.59 ns and $\langle\tau\rangle$ = 2.75 ns. The average lifetime is close to the unquenched value because the quenched residue (τ_1 = 0.5 ns) contributes only f_1 = 0.091 to the steady-state or integrated intensity. If the sample contained two tryptophan residues with equal steady-state intensities, and lifetimes of 5.0 and 0.5 ns then $\bar{\tau} = 0.5(\tau_1) + 0.5(\tau_2)$ = 2.75 ns. The fact that $\langle\tau\rangle$ reflects the relative quantum yield can be seen from noting that $\langle\tau\rangle/\tau_0$ = 2.75/5.0 = 0.55, which is the quantum yield of the quenched sample relative to the unquenched sample.

A4.5. The DAS can be calculated by multiplying the fractional intensities ($f_i(\lambda)$) by the steady-state intensity at each wavelength ($I(\lambda)$). For the global analysis these values (Figure 4.65) match the emission spectra of the individual components. However, for the single-wavelength data the DAS are poorly matched to the individual spectra. This is because the $\alpha_i(\lambda)$ values are not well determined by the data at a single wavelength.

A4.6. The total number of counts in Figure 4.45 can be calculated from the $\alpha\tau$ product. The value of α is the number of counts in the time zero channel or 10^4 counts. The total number of photons counted is thus 4

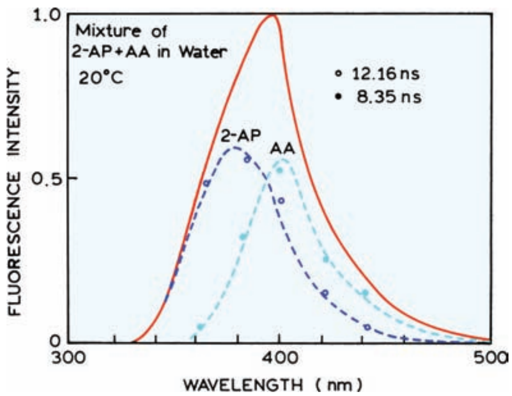

Figure 4.65. Emission spectra of a two-component mixture of anthranilic acid (AA) and 2-aminopurine (2-AP). The data show the fractional amplitudes associated with each decay time recovered from the global analysis. From [187].

x 10^6. Assuming 1 photon is counted each 10^{-5} seconds the data acquisition time is 400 s or 6.7 minutes. If the data were collected by TCSPC with a 1% count rate the data acquisition time would be 670 minutes.

A4.7. For a 4-ns lifetime the excitation pulses should be at least 16 ns apart, which corresponds to a pulse rate of 62.5 MHz. Using a 1% count rate yields a photon detection rate of 0.625 MHz. At this rate the time needed to count 4 x 10^6 photons is 6.4 seconds. Can the TAC convert photons at this rate? The 0.625 MHz count rate corresponds to 1.6 microsecond to store the data. Using a TAC with a 120-ns deadtime the TAC should be able to accept all the photons. A TAC with a 2 μs deadtime would be unable to accept the data and the counting would be inefficient.

A4.8. The fractional intensity is proportional to the $\alpha\tau$ products. Using eq. 4.28, f_1 = 0.9990 and f_2 = 0.001.

CHAPTER 5

A5.1. The decay times can be calculated from either the phase or modulation data at any frequency, using eqs. 5.3 and 5.4. These values are listed in Table 5.7. Since the decay times are approximately equal from phase and modulation, the decay is nearly a single exponential. One expects the decay to become non-exponential at high chloride concentrations due to transient effects in quenching. This effect is not yet visible in the FD data for SPQ.

Table 5.7. Apparent Phase and Modulation Lifetimes for the Chloride Probe SPQ

Chloride concentration	Frequency (MHz)	Apparent phase lifetime (τ_ϕ) (ns)	Apparent modulation lifetime (τ_m) (ns)
0	10	24.90	24.94
	100	24.62	26.49
10 mM	10	11.19	11.07
	100	11.62	11.18
30 mM	10	5.17	5.00
	100	5.24	5.36
70 mM	10	2.64	2.49
	100	2.66	2.27

A5.2. The chloride concentration can be determined from the phase or modulation values of SPQ at any frequency where these values are sensitive to chloride concentration. Examination of Figure 5.15 indicates that this is a rather wide range from 5 to 100 MHz. One can prepare calibration curves of phase or modulation of SPQ versus chloride, as shown in Figure 5.56. An uncertainty of ±0.2° in phase or ±0.5% in modulation

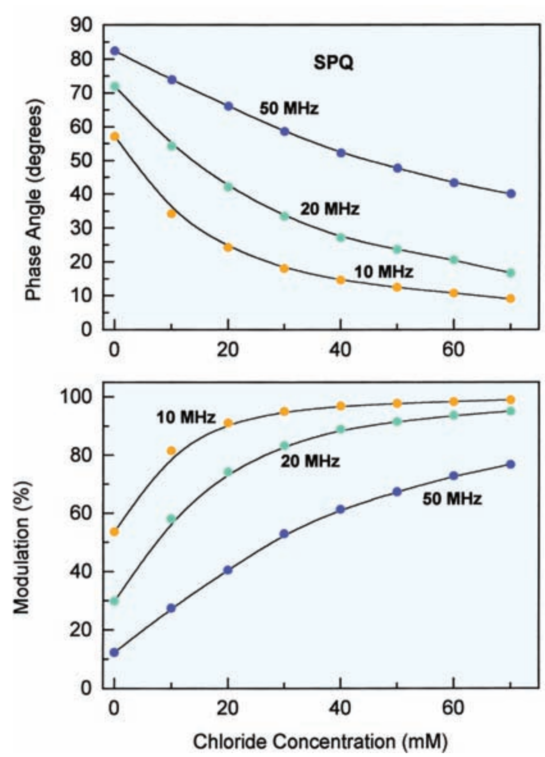

Figure 5.56. Dependence of the phase and modulation of SPQ on chloride concentration.

Table 5.8. Phase-Modulation Apparent Lifetimes for a Double-Exponential Decay[a]

Frequency (MHz)	ϕ (deg)	m	τ_ϕ (ns)	τ_m (ns)
50 ($\alpha_1 = \alpha_2$)	50.5	0.552	3.86	4.81
50 ($f_1 = f_2$)	25.6	0.702	1.53	3.23
100 ($\alpha_1 = \alpha_2$)	60.1	0.333	2.76	4.51
100 ($f_1 = f_2$)	29.8	0.578	0.91	3.17

[a]For both decay laws the lifetimes are 0.5 and 5.0 ns.

results in chloride concentrations accurate to approximately ±0.2 and 0.3 mM respectively, from 0 to 25 mM.

A5.3. A list of the phase and modulation values for the two decay laws, as well as the apparent phase and modulation lifetimes, is given in Table 5.8. As expected, $\tau_\phi^{app} < \tau_m^{app}$. Both values decrease with higher modulation frequency. The phase angles are smaller, and the modulation is higher, when $f_1 = f_2$ than when $\alpha_1 = \alpha_2$. When $f_1 = f_2$, the α_i values are $\alpha_1 = 0.909$ and $\alpha_2 = 0.091$. The fractional contribution of the short-lifetime component is larger when $f_1 = f_2$.

A5.4. The Raman peak at 410 nm is equivalent to 24,390 cm^{-1}. The Raman peak of water is typically shifted 3,600 cm^{-1}. Hence the excitation wavelength is at 27,990 cm^{-1}, or 357 nm.

A5.5. The scattered light has an effective lifetime of zero. Hence the scattered light can be suppressed with $\phi_D = 90°$. The phase angle of quinine sulfate at 10 MHz can be calculated from $\phi = \tan(\omega\tau) = 51.5°$. The maximum phase-sensitive intensity for quinine sulfate would be observed with $\phi_D = 51.5°$. The scattered light is suppressed with $\phi_D = 90°$. At this phase angle the phase-sensitive intensity is attenuated by a factor of $\cos(\phi_D - \phi) = \cos(90 - 51.5) = 0.78$ relative to the phase-sensitive intensity with $\phi_D = 51.5°$.

A5.6. The detector phases of 17.4 + 90° and 32.1 – 90° are out of phase with DNS–BSA and DNS, respectively. This is known because at $\phi_D = 32.1 - 90°$ only free DNS is detected. In the equimolar DNS–BSA mixture the phase-sensitive intensity of DNS is decreased by 50%. Hence 50% of the DNS is bound to BSA. Similarly, at $\phi_D = 17.4 + 90°$ only the fluorescence of the DNS–BSA complex is detected. Relative to the solution in which DNS is completely bound, the intensity is 50%. Hence 50% of the DNS is bound. The phase-sensitive intensities of the first two solutions may be rationalized as follows. Upon addition of a saturating amount of BSA all the DNS is bound. Therefore its contribution to the signal at $\phi_D = 32.1 - 90°$ is eliminated. The intensity increases twofold, and now is observed with $\phi_D = 17.4 + 90°$. However, a twofold increase in intensity is not observed because the signal from the bound DNS is more demodulated than that of the free DNS. Specifically, these values are 0.954 and 0.847 for 5 and 10 ns, respectively. Hence the expected twofold increase in fluorescence intensity is decreased by a factor of 0.847/0.954 = 0.888.

A5.7. The viscosity of propylene glycol changes dramatically with temperature, which affects the rate of solvent relaxation. At an intermediate temperature of –10°C the relaxation time is comparable to the lifetime. Under these conditions the emission spectrum contains components of the unrelaxed initially excited state (F) and the relaxed excited state (R). Suppression on the red side of the emission (410 nm) results in recording the emission spectrum of the F state. Suppression of the blue side of the emission (310 nm) results in recording of the emission spectrum of the R state. Of course, these are only the approximate spectra of these states, but the phase-sensitive spectra appear to show the positions of the unrelaxed and relaxed emission spectra. At very low temperatures (–60°C) all the emission is from the unrelaxed state, and at high temperatures (40°C) all the emission is from the relaxed state. Since there is only one lifetime across the emission spectra, suppression on either side of the emission suppresses the entire emission spectrum.

CHAPTER 6

A6.1. The Stokes shift in cm^{-1} can be calculated from the Lippert equation (eq. 6.17). Because it is easy to confuse the units, this calculation is shown explicitly:

$$\nu_A - \nu_F = \frac{2(0.3098)}{(6.6256x10^{-27})(2.9979x10^{10})} \frac{(14x10^{-18})^2}{(4.0x10^{-8})^3}$$

$$\bar{\nu}_A - \bar{\nu}_F = 9554\,\text{cm}^{-1} \tag{6.23}$$

The emission maximum in the absence of solvent effects is assumed to be 350 nm, which is 28,571 cm^{-1}. The orientation polarizability of methanol is expected to decrease the excited state energy by 9554 cm^{-1}, to 19,017 cm^{-1}, which corresponds to 525.8 nm.

The units for $\bar{\nu}_A - \bar{\nu}_F$ are as follows:

$$\frac{(\text{esu cm})^2}{(\text{ergs})\,(\text{cm/s}(\text{cm}^3)} \tag{6.24}$$

Recalling that erg = g cm^2/s^2 and esu = $g^{1/2}$ $cm^{3/2}/s$, one obtains $\bar{\nu}_A - \bar{\nu}_F$ in cm^{-1}.

A6.2. The change in dipole moment can be estimated from the Lippert plot (Figure 6.53). This plot shows biphasic behavior. In low-polarity solvents the emission is probably due to the LE state, and in higher-polarity solvents the emission is due to the ICT state. The slopes for each region of the Lippert plot are

slope (LE)= 7000 cm^{-1}
slope (ICT) = 33,000 cm^{-1}

The slope is equal to $2(\mu_E - \mu_G)^2/hca^3$. Assuming a radius of 4.2 Å used previously,[42]

$$(\mu_E - \mu_G)^2 = \frac{7000}{2} hca^3 \tag{6.25}$$

$$= \frac{7000}{2}(6.626x10^{-27})(3x10^{10})(4.2x10^{-8})^3 = 5.15x10^{-35}$$

The units of $(\mu_E - \mu_G)^2$ are (cm^{-1}) (erg s)(cm/s)(cm^3). Using erg = g cm^2/s^2, one obtains the units (g cm^3/s^2)(cm^2). Taking the square root yields)

$$\frac{g^{1/2}cm^{3/2}}{s}\,cm \tag{6.26}$$

Since esu = $g^{1/2}$ $cm^{3/2}/s$, the result $(\mu_E - \mu_G)$ is in esu cm. This yields $(\mu_E - \mu_G) = 7.1 \times 10^{-18}$ esu cm = 7.1D. The dipole moment of Prodan is estimated to change by 7.1 Debye units upon excitation. An electron separated from a unit positive charge by 1 Å has a dipole moment of 4.8D. Hence there is only partial charge separation in the LE state. It should be noted that this value is smaller than initially reported[42] due to an trivial error during the calculations.[58]

For the ICT state a similar calculation yields $(\mu_E - \mu_G)^2 = 2.42 \times 10^{-34}$ and $\Delta\mu = 1.56 \times 10^{-17}$ esu cm = 15.6D. This change in dipole moment is equivalent to separation of a unit change by 3.2 Å, which suggests nearly complete charge separation in the ICT state of Prodan.

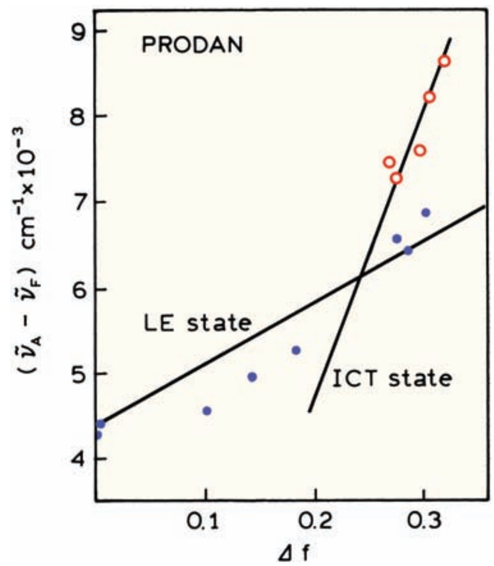

Figure 6.53. Lippert plot of the Stokes shift of Pordan. Data from [42].

CHAPTER 7

A7.1. Assume the decay is a single exponential. Then the time where the intensity has decayed to 37% of its original intensity is the fluorescence lifetime. These values are τ_F = 1 ns at 390 nm and τ = 5 ns at 435 nm. The decay time of 5 ns at 435 nm is the decay time the F-state would display in the absence of relaxation. The lifetime of the F-state at 390 nm is given by $1/\tau_F = 1/\tau + 1/\tau_S$. This is equivalent to stating the decay time of the F-state (γ_F) is equal to the sum of the rates that depopulate the F-state, $\gamma_F = 1/\tau + k_S$. Hence τ_S = 1.25 ns.

A7.2. In the fluid solvents ethanol or dioxane the apparent lifetimes of TNS are independent of wavelength, indicating spectral relaxation is complete in these solvents. In glycerol or DOPC vesicles the apparent lifetimes increase with wavelength, suggesting time-dependent spectral relaxation. The observation of $\tau^{\phi} > \tau^{m}$ at long wavelength is equivalent to observing a negative pre-exponential factor, and proves that relaxation is occurring at a rate comparable to the intensity decay rate.

A7.3. The lifetime of the R state (τ_{OR}) can be calculated from the phase angle difference $\Delta\phi = \phi_R - \phi_F$. At 100 MHz this difference is 58°, which corresponds to a lifetime of 16 ns.

A7.4. A. Acridine and acridinium may be reasonably expected to display distinct absorption spectra. The emission spectrum in 0.2 M NH_4NO_3 (Figure 7.49) shows evidence for emission from both acridine and acridinium. Hence if both species were present in ground state, the absorption spectrum should be a composite of the absorption spectra of acridine and acridinium. In contrast, if the acridinium is formed only in the excited state, then the absorption spectrum in 0.2 M NH_4NO_3 should be almost identical to that of neutral acridine.

B. Examination of the data (Table 7.6) reveals two decay times that are independent of emission wavelength. This indicates that there are two emitting species and that their decay rates are independent of emission wavelength. On the short-wavelength side of the emission the decay is a single exponential. This result indicates the reaction is irreversible and that the measured decay times at other wavelengths contain contributions from both acridine and acridinium. Proof of an excited-state reaction is provided by observation of negative pre-exponential factors. As the observation wavelength is increased this term becomes more predominant. At the longest observation wavelengths one finds that the pre-exponential factors are nearly equal in magnitude and opposite in sign. This near equality of the pre-exponential factors indicates that at 560 nm the emission is predominantly from the relaxed species. The fact that α_2 is slightly larger than α_1 indicates that there is still some emission from neutral acridine at 560 nm.

A7.5. Red-edge excitation selects for fluorophores that are most strongly interacting with the solvent. The solvent configuration around these selected fluorophores is similar to that in a solvent-relaxed state. The TRES with 416-nm excitation do not show a time-dependent shift because the fluorophore is already in the relaxed state.

CHAPTER 8

A8.1. The apparent bimolecular quenching of 2-AP by Cu^{2+} can be found by noting that $F_0/F = 1.10$ at 2 x 10^{-6} M Cu^{2+}. Hence $K = 50{,}000$ M^{-1} and $k_q = 5 \times 10^{12}$ M^{-1} s^{-1}. Similarly, $F_0/F = 1.7$ at 0.001 M DMA, yielding $K = 700$ M^{-1} and $k_q = 7 \times 10^{10}$ M^{-1} s^{-1}. Both values are larger than the maximum value possible for diffusive quenching in water, near 1 x 10^{10} M^{-1} s^{-1}. This implies some binding or localization of the quenchers near the fluorophores.

A8.2. The data in Figure 8.72 can be used to calculate the lifetimes of pyrene, which are 200, 119, and 56 ns in the presence of N_2, air or O_2, respectively. Assuming the oxygen solubility in DMPC vesicles is fivefold larger than in water (0.001275 M/atm in water), the oxygen bimolecular quenching constant is $k_q = 2 \times 10^9$ M^{-1} s^{-1}. This value is about 20% of the value expected for a fluorophore dissolved in water.

A8.3. The data in the absence of benzyl alcohol (Figure 8.73) can be used to calculate a bimolecular quenching constant of 6 x 10^9 M^{-1} s^{-1}. This indicates that the naphthalene is mostly accessible to iodide and probably not bound to the cyclodextrin. This conclusion is supported by the data in the presence of benzyl alcohol. In the presence of benzyl alcohol the Stern-Volmer plots curve downward in the presence of β-CD (Figure 8.74). This suggests the presence of two naphthalene populations, one of which is less accessible to iodide quenching. In the presence of benzyl alcohol and 5.1 mM β-CD the Stern-Volmer plot is still curved, and the apparent value of k_q decreases, which indicates shielding from iodide quenching. Under these conditions it seems that naphthalene binds to β-CD only in the presence of benzyl alcohol.

A8.4. Figure 8.77 shows a plot of F_0/F versus [I^-]. From the upward curvature of this plot it is apparent that both static and dynamic quenching occur for the same population of fluorophores. The dynamic (K_D) and static (K_S) quenching constants can be calculated by a plot of the apparent quenching constant (K_{app}) versus the

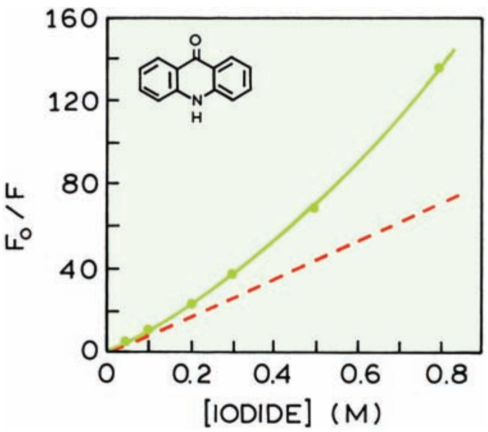

Figure 8.77. Iodide quenching of acridone. Data from [175].

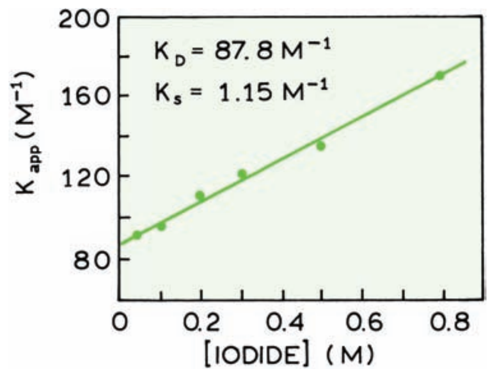

Figure 8.78. Static and dynamic quenching constants of acridone. Data from [175].

concentration of quencher [I^-]. The apparent quenching constant is given by $(F_0/F - 1)/[I^-] = K_{app}$.

M KI	K_{app}
0	–
0.04	91.0
0.10	96.0
0.20	110.0
0.30	121.0
0.5	135.0
0.8	170.0

These results are plotted in Figure 8.78. In the plot the y-intercept is $K_D + K_S = 89$ M^{-1}, and the slope is $K_D K_S = 101$ M^{-2}. The quadratic equation can be solved to find K_D and K_S. Assuming the larger value is K_D we obtain $K_D = 87.8$ M^{-1} and $K_S = 1.15$ M^{-1}. The bimolecular quenching constant is given by $K_D/\tau_0 = k_q = 4.99 \times 10^9$ M^{-1} s^{-1}. The collisional frequency can be calculated independently from the Smoluchowski equation. Assuming a collision radius of 4 Å, and the diffusion of the quencher to be dominant, one obtains

$$k_0 = 4\pi RDN/10^3$$

$$= [(4\pi(4 \times 10^{-8}\text{cm})(2.065 \times 10^{-5}\text{cm}^2/\text{sec})$$

$$(6.02 \times 10^{23}\text{mole}^{-1}))/(10^3\text{cm}^3 l^{-1})]$$

$$= 0.625 \times 10^{10} M^{-1}\text{sec}^{-1} \quad (8.51)$$

This value describes the quenching constant expected if 100% of the collisional encounters are effective in quenching. Hence the quenching efficiency $\gamma = k_q/k_0 = 0.80$.

The radius of the sphere of action can be calculated using any of the F_0/F values for which there is excess quenching. At 0.8 M iodide the expected value of F_0/F due only to dynamic quenching is

$$\left(\frac{F_0}{F}\right)_D = 1 + 87.8(0.8) = 71.24 \quad (8.52)$$

This is indicated by the dashed line in Figure 8.77. The observed value of F_0/F is 137. Using

$$F_0/F = (1 + K_D[Q]) \exp([Q]NV/1000) \quad (8.53)$$

we obtain $\exp([Q]NV/1000) = 1.92$ or $[Q]NV/1000 = 0.653$. From these results one can calculate that the volume of the sphere of action is $V = 1.36 \times 10^{-21}$ cm^3. Using $V = 4/3\ \pi r^3$, where r is the radius, one finds $r = 6.9$ Å. According to this calculation, whenever an iodide ion is within 6.9 Å of an excited acridone molecule the probability of quenching is unity.

The static quenching constant is quite small, as is the radius of the sphere of action. It seems that no actual complex is formed in this case. Rather, the static component is due simply to the probability that a fluorophore is adjacent to a quencher at the moment of excitation.

A8.5. Using the data in Problem 8.5 one may calculate the following:

[AMP] (mM)	τ_0/τ	F_0/F	$(F_0/F)/(\tau_0/\tau)$
0.0	1.0	1.0	1.0
1.75	1.265	1.40	1.107
3.50	1.502	1.80	1.198
5.25	1.741	2.35	1.35
7.0	1.935	3.00	1.55

The collisional or dynamic quenching constant can be calculated from a plot of τ_0/τ versus [AMP] (Figure 8.79). The dynamic quenching constant is 136 M^{-1}. Using the lifetime in the absence of quencher one finds $k_q = K_D/\tau_0 = 4.1 \times 10^9\ M^{-1}\ s^{-1}$, which is typical for a diffusion-controlled reaction which occurs with high efficiency.

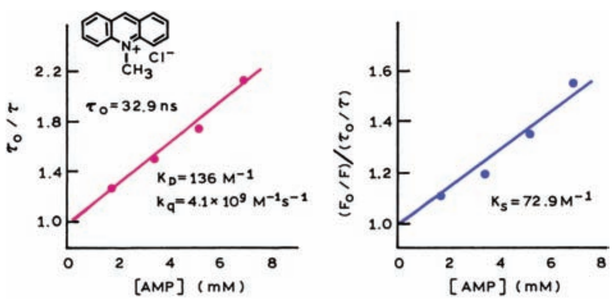

Figure 8.79. Quenching of methylacridinium chloride by AMP. From [18].

In the previous problem we obtained K_S and K_D from a plot of the apparent quenching constant versus quencher concentration (Figure 8.78). In this case both the lifetime and yield data are given, and a simpler procedure is possible. We calculated the quantity $(F_0/F)/(\tau_0/\tau)$. From eqs. 8.8, and 8.19 this quantity is seen to reflect only the static component of the quenching:

$$\frac{F_0/F}{\tau_0/\tau} = 1 + K_S[\text{AMP}] \tag{8.54}$$

A plot of $(F_0/F)/(\tau_0/\tau)$ versus [AMP] yields the association constant as the slope (Figure 8.79).

In contrast to the apparent association constant for the "acridone–iodide complex," this value (72.9 M^{-1}) is much larger. An actual ground-state complex is likely in this case. This was demonstrated experimentally by examination of the absorption spectrum of MAC, which was found to be changed in the presence of AMP. If the MAC–AMP complex is nonfluorescent, then the only emission observed is that from the uncomplexed MAC. Since these molecules are not complexed, the excitation spectrum of MAC in the presence of AMP will be that of MAC alone.

A8.6. The susceptibility of a fluorophore to quenching is proportional to its fluorescence lifetime. Fluorophores with longer lifetimes are more susceptible to quenching. To decide on the upper limit of lifetimes, above which oxygen quenching is significant, we need to consider dissolved oxygen from the air. Based on the assumed accuracy of 3% we can use $F_0/F = \tau_0/\tau = 1.03$. Since the atmosphere is 20% oxygen, the oxygen concentrations due to atmospheric oxygen are one-fifth the total solubility. For aqueous solutions

$$\frac{F_0}{F} = \frac{\tau_0}{\tau} = 1.03 = 1 + k_q\tau_0[O_2] \tag{8.55}$$

Using the information provided for aqueous solutions

$$\tau_0 = \frac{0.03}{k_q[O_2]} = \frac{0.03(5)}{(1 \times 10^{10})(.001275)} = 11.8 \text{ ns} \tag{8.56}$$

For the ethanol solution

$$\tau_0 = \frac{0.03(5)}{(2 \times 10^{10})(.001275)(5)} = 1.2 \text{ ns} \tag{8.57}$$

If the unquenched lifetimes are longer than 1.2 ns in ethanol, or 11.8 ns in water, then dissolved oxygen from the air can result in significant quenching (greater than 3%). If desired this quenching can be minimized by purging with an inert gas, such as nitrogen or argon.

A8.7. The rate of collisional deactivation can be calculated from the decrease in lifetime due to collisions with the adenine ring. The lifetimes in the absence (τ_0) and presence of (τ) of the adenine moiety are $\tau_0 = \gamma^{-1}$ and $\tau = (\gamma + k)^{-1}$. Therefore,

$$k = \frac{1}{\tau} - \frac{1}{\tau_0} = 2.0 \times 10^8\,\text{s}^{-1} \tag{8.58}$$

The quantum yield of FAD is decreased by both static and dynamic quenching:

$$\frac{F}{F_0} = \frac{Q(\text{FAD})}{Q(\text{FMN})} = f\frac{\tau}{\tau_0} \tag{8.59}$$

where f is the fraction not complexed. Hence

$$f = \frac{\tau_0\, Q(\text{FAD})}{\tau\, Q(\text{FMN})} = \frac{(4.6)(0.09)}{(2.4)(1.0)} = 0.17 \quad (8.60)$$

83% of the FAD exists as a nonfluorescent complex.

A8.8. Using the data provided one can calculate the following quantities needed for the Stern-Volmer plots:

$[I^-]$, M	F_0/F	ΔF	$F_0/\Delta F$	$[I^-]^{-1}$, M^{-1}
0.0	1.000	0	–	–
0.01	1.080	0.074	13.51	100
0.03	1.208	0.172	5.814	33.3
0.05	1.304	0.233	4.292	20.0
0.10	1.466	0.318	3.145	10.0
0.20	1.637	0.389	2.571	5.0
0.40	1.776	0.437	2.288	2.5

The downward curvature of the Stern-Volmer plot indicates an inaccessible fraction (Figure 8.80). From the intercept on the modified Stern-Volmer plot one finds $f_a = 0.5$. Hence one tryptophan residue per subunit is accessible to iodide quenching. The slope on the modified Stern-Volmer plot is equal to $(f_a K)^{-1}$. Thus $K = 17.4\ M^{-1}$. By assumption, the quenching constant of the inaccessible fraction is zero using these results one can predict the quenching plots for each tryptophan residue.

$[I^-]$, M	$[I^-]^{-1}$, M^{-1}	$(F_0/F)_b$	$(F_0/F)_a$+	$(F_0/F)_b$	$(F_0/\Delta F)_a$++
0.0	0	1.0	1.0	–	–
0.01	100	"	1.174	"	6.747
0.03	33.3	"	1.522	"	2.916
0.05	20.0	"	1.870	"	2.149
0.10	10.0	"	2.740	"	1.575
0.20	5.0	"	4.480	"	1.287
0.40	2.5	"	7.96	"	1.144

+Calculated from $F_0/F = 1 + 17.4\ [I^-]$.
++Calculated from $F_0/\Delta F = 1/K[Q] + 1$.

For the accessible fraction the Stern-Volmer plot is linear and the apparent value of $f_a = 1$ (Figure 8.81). Hence if the quenching data were obtained using 300-nm excitation, where only the accessible residue was excited, all the fluorescence would appear to be accessible. Since the inaccessible fraction is not quenched, $F_0/F = 1$ for this fraction. One cannot construct a modified Stern-Volmer plot since $\Delta F = 0$ for this fraction. The bimolecular quenching constant can be calculated using $K = 17.4\ M^{-1}$ and $\tau = 5$ ns, yielding a bimolecular quenching constant $k_q = 0.35 \times 10^{10}\ M^{-1}\ s^{-1}$.

A8.9. Quenching of Endo III by poly(dAdT) displays saturation near 20 μM, which indicates specific binding of

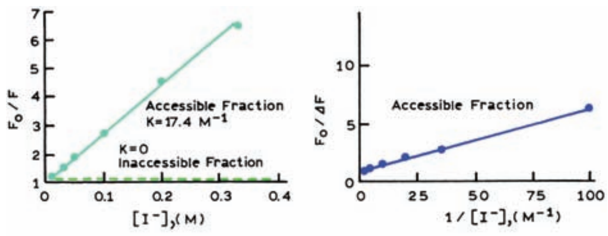

Figure 8.80. Predicted Stern-Volmer plots for the accessible and inaccessible tryptophan residues.

poly(dAdT) to Endo III. Assume the quenching is dynamic. Then K_D is near $10^5\ M^{-1}$, resulting in an apparent value of $k_q = 2 \times 10^{13}\ M^{-1}\ s^{-1}$. This is much larger than the diffusion controlled limit, so there must be some specific binding.

About 50% of the fluorescence is quenched. In Section 8.9.1 we saw that both residues were equally fluorescent. Hence the titration data (Figure 8.75) suggests that one residue, probably 132, is completely quenched when poly(dAdT) binds to Endo III.

A8.10. The structure of wild-type tet repressor is shown in Figure 8.39. The W75F mutant contains a phenylalanine in place of Trp 75, and thus only one Trp at position 43. This tryptophan is immediately adjacent to bound DNA, which quenches the Trp 43 emission. The extent of quenching is over 50% because there is only one type of tryptophan. The wild-type protein would be expected to show less quenching because Trp 75 will probably not be quenched by DNA.

A8.11. The relative intensities can be calculated from the Stern-Volmer equation:

$$\frac{F_0}{F} = \frac{\tau_0}{\tau} = 1 + k_q \tau_0 \quad (8.61)$$

For DBO with a lifetime of 120 ns, and $k_q = 9 \times 10^6\ s^{-1}$, the relative intensity is $F/F_0 = 0.48$. The DBO is about 50% quenched. For $\tau_0 = 2$ ns, $F/F_0 = 0.98$ and the quenching would probably not be detectable. For $\tau_0 = 2$ ms, $F/F_0 = 5.6 \times 10^{-5}$ and the fluorophore would be completely quenched.

CHAPTER 9

A9.1. In order for PET to occur $\Delta G < 0$. We can use the Rehm-Weller equation to estimate the oxidation potential of donor fluorophore if the other quantities are known. The $S_0 \otimes S_1$ wavelength of 365 nm corresponds to 3.4 eV (eqs. 9.11 and 9.12). Using $\Delta G < 0$ and eq. 9.10 yields $E(D^+/D) \otimes 3$ V. Hence it requires more than 69.2 kcal/mole to oxidize the fluorophore. If more than 3 volts were required to remove an electron from the fluorophore then PET would not occur. It is difficult to intuitively understand the sign of $E(D^+/D)$ because of the convention that $\Delta E > 0$ corresponds to $\Delta G < 0$.

A9.2. Methylation of the pyridine results in a greater affinity for electrons. Hence PET from the fluorophore occurs to the pyridinium group but not to the more electron-rich pyridine group.

CHAPTER 10

A10.1. At 430, 290, and 270 nm the r_0 values of perylene are near 0.38, 0.10, and 0.0, respectively. The angle β between the absorption and emission moments can be calculated using eq. 10.22. These calculations yield β = 16.8, 45, and 54.7°, respectively.

A10.2. If the sample is weakly scattering, the scattered component will be completely polarized (r = 1.0). The measured anisotropy can be obtained using eq. 10.6

$$r_{obs} = 0.30(0.80) + 1.0(0.20) = 0.44 \quad (10.53)$$

The anisotropy above 0.40 should be an immediate warning that the measured value was not due only to fluorescence.

A10.3. The corrected ratio, I_{VV}/I_{HV}, is given by 1.33/0.45 = 2.96. Therefore r_0 = 0.395 and P_0 = 0.495. The angle between the absorption and emission dipoles can be calculated using eq. 10.22. Substitution of r_0 = 0.395 yields β = 5.2°.

A10.4. The denominator in eq. 10.43 is given by

$$\int_0^\infty I(t)\,dt = I_0 \int_0^\infty \exp(-t/\tau)\,dt = I_0\tau \quad (10.54)$$

The numerator in eq. 10.43 is given by

$$\int_0^\infty I(t)r(t)\,dt = \int_0^\infty \exp\left[-t\left(\frac{1}{\tau}+\frac{1}{\theta}\right)\right]dt = I_0 r_0 \frac{\tau\theta}{\tau+\theta} \quad (10.55)$$

Division of eq. 10.55 by 10.54 yields eq. 10.44.

A10.5. The rotational correlation time of perylene can be calculated using eq. 10.46:

$$\theta = \frac{\eta V}{RT} = \frac{(0.01194\ P)(252\ \text{g/mole})(0.74\ \text{ml/g})}{(293°\text{K})(8.314 \times 10^7 \text{erg/mole °K})} \quad (10.56)$$

$$\theta = 91\ \text{ps} \quad (10.57)$$

The anisotropy can be calculated using eq. 10.44:

$$r = \frac{0.36}{1 + 6/0.091} = 0.005 \quad (10.58)$$

A similar calculation for propylene glycol at 25°C yields θ = 2.4 ns and r = 0.103.

A10.6. Equation 10.51 can be derived by reasoning an expression for the average anisotropy. Suppose the quantum yield of the free and bound forms are q_F and q_B, respectively. Then the measured anisotropy is

$$r = \frac{f_F q_F r_F + f_B q_B r_B}{f_F q_F + f_B q_B} \quad (10.59)$$

The correctness of this expression can be seen by noting the numerator is simply a revised form of the additivity law for anisotropies, and the products $f_F q_F$ and $f_B q_B$ represent the intensities of each form of the probe. The denominator normalizes these values to fractional fluorescence intensities. Equation 10.59 can be rearranged to eq. 10.51 by noting $f_F + f_B$ = 1.0 and $R = q_B/q_F$. Setting R = 1 yields eq. 10.50.

A10.7. A. The observed polarizations may be converted into anisotropies using $r = 2P/(3 - P)$. The latter are more convenient since

$$\bar{r} = f_F r_F + f_B r_B \quad (10.60)$$

where the subscripts F and B represent the free and bound forms of the fluorophore, and f_i is the fraction of fluorescence due to each form of the probe. When [BSA] = 0 one observes r_F, and when [BSA] >> K_d one observes r_B. These considerations are summarized below:

[BSA]	Observable	r
0	r_F	0.010
2 x 10^{-5} M	r	0.200
>> K_d	r_B	0.300

Using eq. 10.59 one obtains

$$0.20 = f_F(0.01) + (1 - f_F)(0.30) \quad (10.61)$$

and hence $f_F = 0.345$ and $f_B = 0.655$. Since the concentration of DNS is much less than that of BSA, we can assume that the concentration of unliganded BSA is not depleted by the binding of DNS. The ratio of free to bound DNS is given by 0.345/0.655. Hence from eq. 10.52:

$$K_d = \frac{(2 \times 10^{-5}\ \text{M})(0.345)}{(0.655)} = 1.05 \times 10^{-5}\ \text{M} \quad (10.62)$$

B. In the use of eq. 10.60 we assumed that the calculated fractional intensity of each species represented the fraction of the DNS which was bound and free. However, if the relative quantum yield of the bound probe is twofold larger than the free probe, then clearly the concentration of the bound form is twofold lower. Therefore:

$$K_d = \frac{(2 \times 10^{-5}\ \text{M})(0.345)}{(0.655)/2} = 2.1 \times 10^{-5}\ \text{M} \quad (10.63)$$

C. A change in quantum yield could be readily detected by comparing the intensity of the DNS solution, with and without added BSA. Since the DNS concentrations are identical the relative intensities represent the relative quantum yields.

D. Using the data provided, the calculated rotational correlation time of BSA is 20 ns. The anisotropy of free DNS will decay too rapidly for measurement with most currently available instruments. For the solution containing a concentration of BSA adequate to bind all the DNS one expects

$$r(t) = 0.20\, e^{-t/20} \quad (10.64)$$

For the 2 x 10^{-5} M solution

$$r(t) = f_B r_0 e^{-t/20} = 0.131\, e^{-t/20} \quad (10.65)$$

CHAPTER 11

A.11.1. The angle can be calculated using eq. 11.51. Using an apparent time of 0, an anisotropy of 0.22, as r_∞, one finds $<\cos^2 \theta> = 0.924$ and $\theta = 16°$.

A.11.2. The most direct approach is to use the amplitudes from the intensity decay. The radiative rate of a fluorophore is usually not affected by its environment. Hence, the relative values of α_i represent the fraction of the FMN free or bound to YFP. The dissociation constant is given by

$$K_d = \frac{[\text{FMN}][\text{YFP}]}{[\text{FMN}\,.\,\text{YFP}]} \quad (11.52)$$

This equation can be rewritten in terms of the total YFP concentration and the fraction of FMN bound (f_B):

$$K_d = \frac{[\text{YFP}]_\tau (1 - f_B)^2}{f_B} \quad (11.53)$$

where $[\text{YFP}]_\tau$ = [YFP] + [FMN·YFP] is the total concentration of YFP. This expression can be understood by noticing that the concentrations of free YFP and FMN are both given by $[\text{YFP}]_T(1 - f_B)$, and that the concentration of [FMN·YFP] = $[\text{YFP}]_T f_B$. At [YFP] = 0.18 μM the fraction bound is given by

$$f_B = \frac{\alpha_2}{\alpha_1 + \alpha_2} = 0.31 \quad (11.54)$$

Hence, $K_d = 0.28 \times 10^{-6}$ M.

CHAPTER 12

A12.1. The anisotropy of any time can be calculated using eq. 12.1. These values are listed in Table 12.3. The

Table 12.3. Associated Anisotropy Decay

t (ns)	$f_1(t)$	$f_2(t)$	$r_1(t)$	$r_2(t)$	$r(t)$
0	0.5	0.5	0.3	0.3	0.30
1	0.45	0.55	0.0	0.29	0.16
5	0.25	0.75	0.0	0.27	0.20

anisotropy values for the non-associated decay can be calculated using

$$r(t) = r_0[0.5 \exp(-t/0.05) + 0.5 \exp(-t/40)] \quad (12.51)$$

For t = 0, 1, and 5 ns these values are 0.30, 0.146, and 0.132, respectively.

The presence of an associated anisotropy decay can be seen from the increase in anisotropy at 5 ns as compared to 1 ns. For the non-associated decay the anisotropy decreases monotonically with time.

A12.2. For a non-associative model the anisotropy decay is given by

$$r(t) = r_0[g_1 \exp(-t/\theta_1) + g_2 \exp(-t/\theta_2)] \quad (12.52)$$

where subscripts 1 and 2 refer to components in the decay, not the location of the fluorophore. From Figure 12.5 the time-zero anisotropy appears to be about 0.32. Using the parameter values in this figure,

$$r(t) = 0.32[0.7 \exp(-t/0.30) + 0.3 \exp(-t/685) \quad (12.53)$$

A plot of $r(t)$ would show a rapid decrease to 30% of the time-zero value followed by a long tail where the anisotropy does not decay during the lifetime of the fluorophore.

A12.3. The anisotropy can be calculated using eqs. 10.6 and 10.22. The anisotropy from the three transitions can be calculated using $\beta = 0°$ and $\pm 120°$. Hence, r = 0.33(0.40) + 0.33(–0.05) + 0.33(–0.05) = 0.10.

A12.4. The apparent $r(0)$ values of melittin are near 0.16, which is considerably less than r_0 = 0.26. This indicates that the tryptophan residue in melittin displays fast motions that are not resolved with the available range of lifetimes (0.6 to 2.4 ns).

The apparent correlation times from melittin can be calculated from the slopes in Figure 12.41. For example, in the absence of NaCl the slope is near 5.8 x 10^9, which is equal to $(r(0)\theta)^{-1}$. Hence the apparent correlation time is 1.08 ns.

CHAPTER 13

A13.1. The D–A distance can be calculated using eq. 13.12. The transfer efficiency is 90%. Hence the D–A distance is $r = (0.11)^{1/6}R_0 = 0.69R_0$ = 17.9 Å. The donor lifetime in the D–A pair can be calculated from eq. 13.14, which can be rearranged to $\tau_{DA} = (1 - E)\tau_D$ = 0.68 ns.

A13.2. The equations relating the donor intensity to the transfer efficiency can be derived by recalling the expressions for relative quantum yields and lifetimes. The relative intensities and lifetimes are given by

$$F_D = \frac{\Gamma_D}{\Gamma_D + k_{nr}}, \quad \tau_D = \frac{1}{\Gamma_D + k_{nr}} \quad (13.34)$$

$$F_{DA} = \frac{\Gamma_D}{\Gamma_D + k_{nr} + k_T}, \quad \tau_{DA} = \frac{1}{\Gamma_D + k_{nr} + k_T} \quad (13.35)$$

where Γ_D is the emission rate of the donor and k_{nr} is the non-radiative decay rate. The ratio of intensities is given by

$$\frac{F_{DA}}{F_D} = \frac{\Gamma_D + k_{nr}}{\Gamma_D + k_{nr} + k_T} = \frac{\tau_D^{-1}}{\tau_D^{-1} + k_T} \quad (13.36)$$

Hence

$$1 - \frac{F_{DA}}{F_D} = \frac{k_T}{\tau_D^{-1} + k_T} = E \quad (13.37)$$

One can derive a similar expression for the transfer efficiency E based on lifetime using the right-hand side of eqs. 13.34 and 13.35.

It should be noted that k_T was assumed to be a single value, which is equivalent to assuming a single distance. We also assumed that the donor population was homogeneous, so that each donor had a nearby acceptor, that is, labeling by acceptor is 100%.

A13.3. The excitation spectra reveal the efficiency of energy transfer by showing the extent to which the excitation of the naphthyl donor at 290 nm results in dansyl emission. The transfer efficiency can be calculated from the emission intensity at 450 nm for 290-nm excitation, which reflects acceptor emission due to excitation of the donor and direct excitation of the acceptor. Dansyl-L-propyl-hydrazide does not contain a donor, and hence this excitation spectrum defines that expected for 0% transfer. For dansyl-L-propyl-α-naphthyl, in which the donor and acceptor are closely spaced, energy transfer is 100% efficient. For this donor–acceptor pair the greatest sensitivity of the excitation spectrum to energy transfer is seen near 290 nm, the absorption maximum of the naphthyl donor. For the other derivatives the intensity is intermediate and dependent upon the length of the spacer. For 290-nm excitation the transfer efficiency can be calculated from the relative intensity between 0 and 100% transfer. The efficiency of energy transfer decreases as the length of the spacer is increased.

The object of these experiments was to determine the distance dependence of radiationless energy transfer. Hence we assume that the efficiency of energy transfer depends on distance according to

$$E = \frac{(R_0/r)^j}{(R_0/r)^j + 1} \tag{13.38}$$

where R_0 and r have their usual meanings, and j is an exponent to be determined from the observed dependence of E on r. Rearrangement of eq. 13.38 yields

$$\ln(E^{-1} - 1) = j \ln r - j \ln R_0 \tag{13.39}$$

Hence a plot of $\ln(E^{-1} - 1)$ versus $\ln r$ has a slope of j. These data are shown in Figure 13.41. The slope was found to be 5.9 ± 0.3.[18] From this agreement with the predicted value of $j = 6$ these workers concluded that energy transfer followed the predictions of Förster. See [18] for additional details.

The value of R_0 can be found from the distance at which the transfer efficiency is 50%. From Figure 13.41 (right) R_0 is seen to be near 33 Å.

A13.4. The lifetime of compound I is τ_{DA} and the lifetime of compound II is τ_D. Compound II serves as a control for the effect of solvent on the lifetime of the indole moiety, in the absence of energy transfer. The rate of energy transfer is given by $k_T = \tau_{DA}^{-1} - \tau_D^{-1}$.

$$k_T = CJ \tag{13.40}$$

where C is a constant. Hence a plot of k_T versus J should be linear. The plot of k_T vs. J is shown in Figure 13.42. The slope is 1.10. These data confirm the expected dependence of k_T on the overlap integral. See [20] for additional details.

A13.5. If the wavelength (λ) is expressed in nm, the overlap integral for Figure 13.9 can be calculated using eq. 13.3 and is found to be 4.4×10^{13} M^{-1} cm^{-1} $(nm)^4$. Using eq. 13.5, with $n = 1.33$ and $Q_D = 0.21$, one finds $R_0 = 23.6$ Å. If λ is expressed in cm then $J(\lambda) = 4.4 \times 10^{-15}$ M^{-1} cm^3, and using eq. 13.8 yields $R_0 = 23.6$ Å.

A13.6. The disassociation reaction of cAMP (A) from protein kinase (PK) is described by

$$\text{PK.cAMP} \rightleftharpoons \text{PK} + \text{cAMP}$$

$$B \rightleftharpoons F + A \tag{13.41}$$

where B represents PK with bound cAMP, F the PK without bound cAMP, and A the concentration of

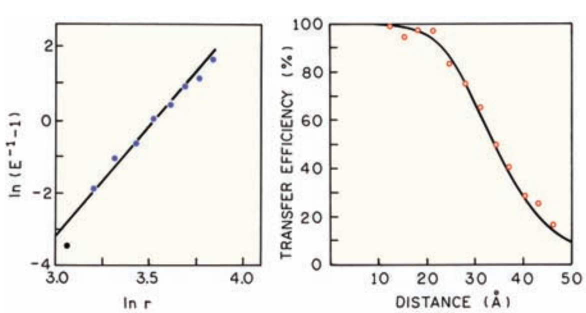

Figure 13.41. Distance dependence of the energy transfer efficiencies in dansyl-(L-propyl)$_n$-α-naphthyl; n = 1–12. Revised from [18].

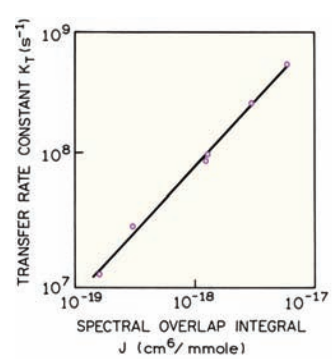

Figure 13.42. Dependence of the rate of energy transfer on the magnitude of the overlap integral. Revised from [20].

cAMP. The dissociation constant for cAMP is defined by

$$K_D = \frac{[F][A]}{[B]} \tag{13.42}$$

Using conservation of mass, $[F] + [B] = [T]$ is the total protein kinase concentration, and one can show the bound and free fractions of PK are given by

$$f_B = \frac{[B]}{[T]} = \frac{[A]}{K_D + [A]}, \quad f_F = \frac{[F]}{[T]} = \frac{K_D}{K_D + [A]} \tag{13.43}$$

Let R_B and R_F represent the intensity ratio of each species. At any given cAMP concentration the observed ratio R is

$$R = f_B R_B + f_F R_F \tag{13.44}$$

Assuming that $f_B + f_F = 1.0$, one obtains

$$[A] = [\text{cAMP}] = K_D\left(\frac{R - R_F}{R_B - R}\right) \tag{13.45}$$

A ratio of intensities is independent of the total PK concentration, and independent of sample-to-sample variations in PK concentration. Hence intensity ratiometric measurements are convenient and accurate. See [99] for additional details.

A13.7. A. The efficiency of energy transfer can be calculated from eq. 13.13:

$$E = 1 - \frac{4.1}{20.5} = 0.80 \tag{13.46}$$

B. The expected lifetime in the presence of DNP can be calculated using eq. 13.14 with $\tau_D = 5.0$ ns and $E = 0.8$:

$$\tau_{DA} = \tau_D(1-E) = 1 \text{ ns} \tag{13.47}$$

C. The rate of energy transfer (k_T) can be calculated using eq. 13.11 with $E = 0.8$ and $\tau_D = 5$ ns:

$$k_T = \frac{E\tau_D^{-1}}{1 - E} = 8 \times 10^8 \text{ s}^{-1} \tag{13.48}$$

D. The distance can be calculated using eq. 13.12. Substitution and rearrangement yields, $r^6 = 0.20\, R_0^6$, and therefore $r = 38.2$ Å.

E. The efficiency can be calculated using eq. 13.12 with $r = 20$ Å. The efficiency is 0.9959. Once the efficiency is known the intensity can be calculated using eq. 13.13. The fluorescence intensity (F_{DA}) is expected to be 0.0041 $F_D = 0.0841$.

F. The 1% impurity would contribute 1% of 20.5, or 0.205 to the total intensity. The contribution from this minor component would be (0.205/0.0841) = 2.44-fold more intense than the signal from the DNP-binding protein, and would invalidate any interpretation of the intensity in the presence of DNP.

G. The lifetime of the sample would be dominated by the impurity and thus would be near 5 ns. Such a result is indicative of an impurity. Specifically, the yield is decreased to 0.0041 of the original value, but the lifetime is relatively unchanged. When this result is found one should consider the presence of a fluorescent impurity.

A13.8. In order to calculate the possible effects of κ^2 on distance we need to determine the depolarization factors due to segmental motion of the donor and acceptor. Knowledge of the rotational correlation time of the protein (θ) allows us to account for this component in the steady state anisotropy. The depolarization factors due to overall rotation (d_{pi}) can be calculated from the Perrin equation. For the donor ($\tau_D = 5$ ns) and acceptor ($\tau_A = 15$ ns) these factors are

$$d_{PD} = \frac{1}{1 + \tau_D/\theta} = 0.5 \tag{13.49}$$

$$d_{PA} = \frac{1}{1 + \tau_A/\theta} = 0.25 \tag{13.50}$$

Recall that the overall depolarization is given by Soleillet's rule (Chapter 10), $r = r_0\, d_{pi}\, d_{si}$, where d_{si} is the factor due to segmental motions of the donor or acceptor. Hence we can use the steady-state anisotropies and calculate the depolarization factors due to rapid segmental probe motions:

$$d_D^x = \left(\frac{r_D}{r_0 d_{PD}}\right)^{1/2} = 0.71 \tag{13.51}$$

$$d_A^x = \left(\frac{r_A}{r_0 d_{PA}}\right)^{1/2} = 0.71 \quad (13.52)$$

Hence the maximum and minimum values of κ^2 are 0.19 and 2.62 (eqs. 13.18 and 13.19). According to eqs. 13.23 and 13.24, the D–A distance can range from $0.81R_0$ to $1.26R_0$, or from 20.3 to 31.5 Å.

A13.9. If f_A = 1.0 then the transfer efficiency is given by eq. 13.13:

$$E = 1 - \frac{0.5}{1.0} = 0.5 \quad (13.53)$$

and the D–A distance is thus equal to R_0. If f_A = 0.5 the transfer efficiency is given by eq. 13.17:

$$E = 1 - \frac{0.5 - 1.0(0.5)}{1.0(0.5)} = 1.0 \quad (13.54)$$

If f_A = 0.5 then the transfer efficiency for the actual D–A pair is 100%, and thus the D–A distance is less than $0.5R_0$. The presence of acceptor underlabeling results in a higher intensity for the presumed D–A pair and an overestimation of the true D–A distance.

A13.10. Equation 13.25 can be easily derived by writing expression for the acceptor intensity. In the absence (F_A) and presence of donor (F_{AD}) the intensities are given by

$$F_A(\lambda_A^{em}) = \varepsilon_A(\lambda_D^{ex}) C_A(\lambda_A^{em}) \quad (13.55)$$

$$F_{AD}(\lambda_A^{em}) = [\varepsilon_A(\lambda_D^{ex}) + E\varepsilon_D(\lambda_D^{ex})] C_A(\lambda_A^{em}) \quad (13.56)$$

where excitation is at λ_D, intensities are measured at λ_A, and E is the transfer efficiency. $C_A(\lambda_A{}^{em})$ is a constant relating the intensity at λ_A to the acceptor concentration. Dividing 13.55 by 13.56, followed by rearrangement, yields eq. 13.25.

If the extent of donor labeling is less than 1.0, then the acceptor intensities are given by

$$F_A(\lambda_A^{em}) = \varepsilon_A(\lambda_D^{ex}) C_A(\lambda_A^{em}) \quad (13.57)$$

$$F_A(\lambda_A^{em}) = [\varepsilon_A(\lambda_D^{ex}) + f_D E\varepsilon_D(\lambda_D^{ex})] C_A(\lambda_A^{em}) \quad (13.58)$$

where f_D is the fractional labeling with the donor. These expressions can be understood by recognizing that the directly excited acceptor intensity is independent of f_D, but the acceptor intensity due to energy transfer depends on f_D. Rearrangement of eqs. 13.57 and 13.58 yields 13.25.

A13.11. Let $C_A(\lambda_A)$ and $C_D(\lambda_A)$ be the constants relating the intensities at λ_A to the acceptor and donor concentrations, respectively, when both are excited at λ_D. Since the donor is assumed to emit at λ_A, eqs. 13.55 and 13.56 become

$$F_A(\lambda_A) = \varepsilon_A(\lambda_D) C_A(\lambda_A) \quad (13.59)$$

$$F_{AD}(\lambda_A) = [\varepsilon_A(\lambda_D) + E\varepsilon_D(\lambda_D)] C_A(\lambda_A) + \varepsilon_D(\lambda_D) C_{DA}(\lambda_A) \quad (13.60)$$

In eq. 13.58 we considered the contribution of the donor in the D–A pair to the intensity at λ_A. In general $C_{DA}(\lambda_A)$ will be smaller than $C_D(\lambda_A)$ due to FRET quenching of the donor. However, $C_D(\lambda_A)$ can be measured with the donor-alone sample. $C_{DA}(\lambda_A)$ can be estimated using the shape of the donor emission to estimate the donor contribution at λ_A in the doubly labeled sample. Eqs. 13.59 and 13.60 can be rearranged to

$$\frac{F_{AD}(\lambda_A)}{F_D(\lambda_D)} - 1 = \frac{E\varepsilon_D(\lambda_D)}{\varepsilon_A(\lambda_D)} + \frac{\varepsilon_D(\lambda_D) C_{DA}(\lambda_A)}{\varepsilon_A(\lambda_D) C_A(\lambda_A)} \quad (13.61)$$

The transfer efficiency as seen from the acceptor emission is given by eq. 13.25, which assumes that the donor does not emit at the acceptor wavelength. Hence the acceptor emission increases the apparent efficiency to

$$E_{app} = E + \frac{C_{DA}(\lambda_A)}{C_A(\lambda_A)} \quad (13.62)$$

and would thus be larger than the actual efficiency. If the donor does not contribute at λ_A, then $C_{DA}(\lambda_A) = 0$

and E_{app} becomes the true efficiency. See [83] for additional details.

A13.12. The true transfer efficiency is defined by the proportion of donors that transfer energy to the acceptor, and is given by

$$E = \frac{k_T}{\tau_D^{-1} + k_q + k_T} \quad (13.63)$$

The apparent efficiency seen for the donor fluorescence is given by

$$E_D = \frac{k_T + k_q}{\tau_D^{-1} + k_q + k_T} \quad (13.64)$$

The apparent efficiency (E_D) is larger than the true efficiency (E) because the additional quenching pathway decreases the donor emission more than would have occurred by FRET alone. See [56] for additional details.

CHAPTER 14

A14.1. The intensity decays of A and C would both be single exponential, but the intensity decay of B would be a triple exponential. For sample A the donors are at a unique distance from acceptors at 15, 20, and 25 Å. The transfer rate is given by

$$k_T = \frac{1}{\tau_D}\left(\frac{20}{15}\right)^6 + \frac{1}{\tau_D}\left(\frac{20}{20}\right)^6 + \frac{1}{\tau_D}\left(\frac{20}{25}\right)^6 \quad (14.27)$$

Calculation of the transfer rate yields $k_T = 6.88\tau_D^{-1}$. Hence the decay of sample A is given by eq. 14.1 and is a single exponential with

$$I_{DA}(t) = \exp\left[-\frac{t}{\tau_D} - \frac{t6.88}{\tau_D}\right] = \exp\left(-\frac{t}{0.63}\right) \quad (14.28)$$

The intensity decay of sample C would be the same single exponential with the same decay time of 0.63 ns.

The intensity decay of sample B would be a triple exponential. There would be three different decay times, which can be calculated from the three transfer rates in eq. 14.28. The decay times are 0.76, 2.5, and 3.96 ns.

A14.2. Since the unquenched lifetime and quantum yields of the three proteins in sample B are the same, the radiative decay rates are the same and the relative amplitude of the three proteins would be the same. Hence the intensity decay would be given by

$$I(t) = \sum_i \alpha_i e^{-t/\tau_D} \quad (14.29)$$

with $\alpha_1 = \alpha_2 = \alpha_3 = 0.33$ and $\tau_1 = 0.76$, $\tau_2 = 2.5$ and $\tau_3 = 3.96$ ns.

In contrast to the α_i values, the fractional intensities will be very different for each protein in sample B. These values are given by

$$f_i = \frac{\alpha_i \tau_i}{\sum_j \alpha_j \tau_j} \quad (14.30)$$

Hence the fractional intensities of the three proteins are 0.105, 0.346, and 0.549.

A14.3. The presence of three acceptors could not be detected in sample A. This is because the only observable would be the decreased donor quantum yield or lifetime. The only way the three acceptors could be detected is from the absorption spectrum, assuming one knows the extinction coefficient for a single acceptor.

A14.4. The apparent distance for an assumed single acceptor can be found from eq. 14.2. Numerically we found $k_T = 6.88\ \tau_D^{-1}$, which can be equated to an apparent distance:

$$k_T = \frac{6.88}{\tau_D} = \frac{1}{\tau_D}\left(\frac{R_0}{r_{app}}\right)^6 \quad (14.31)$$

Solving for r_{app} yields $R_0/r_{app} = 1.38$, so $r_{app} = 14.5$ Å. The extent of energy transfer is thus seen to be dominated by the closest acceptor at 15 Å. The presence of two more acceptors at 20 and 25 Å only decreases the apparent distance by 0.5 Å.

A.14.5. A. One acceptor per 60-Å cube corresponds to an acceptor concentration of 8 mM. Use of eq. 13.33 with $R_0 = 30$ Å yields a critical concentration of 17 mM.

B. A covalently linked acceptor is somewhat equivalent to one acceptor per sphere of 30 Å, or 8.84 x 10^{18} acceptors/cm^3. This is equivalent to an acceptor concentration of 15 mM. Covalent attachment of an acceptor results in a high effective acceptor concentration.

CHAPTER 15

A.15.1. Using the data provided in Figure 15.28 one can calculate the following values:

Mole% Rh-PE	Rh-PE/Å^2	Rh-PE/R_0^2	F_{DA}/F_D
0.0	0.0	0.0	1.0
0.2	2.8 x 10^{-5}	0.071	0.62
0.4	5.7 x 10^{-5}	0.143	0.40
0.8	11.4 x 10^{-5}	0.286	0.21
1.2	17.1 x 10^{-5}	0.429	0.15

The distance of closest approach can be estimated by plotting the last two columns of this table on the simulations shown in Figure 15.17. The observed energy transfer quenching is greater than predicted for no excluded area, $r_C = 0$, or much less than R_0. This suggests that the donors and acceptors are fully accessible and probably clustered in the PE vesicles. The R_0 value was not reported in [64].

A15.2. The decay times can be used with eq. 15.20 to obtain the transfer rate k_T = 1.81 x 10^3 s^{-1}. Dividing by the EB concentration (2.77 μM) yields k_T^b = 6.5 x 10^8 M^{-1} s^{-1}.

Using eq. 15.25 and the values of R_0 and r_C, the maximum bimolecular rate constant is 1.1 x 10^6 M^{-1} s^{-1}. The measured values could be larger than the theoretical values for two reasons. The positively charged donors may localize around the negatively charged DNA. This results in a larger apparent concentration of EB. Given the small value of r_C we cannot exclude the possibility of an exchange contribution to k_T^b.

A15.3. To a first approximation the donor intensity is about 50% quenched when C/C_0 = 0.5. This value of C/C_0 can be used to calculate the acceptor concentration in any desired units, as listed in Table 15.3.

Acceptor concentrations near 2 mM are needed in homogeneous solution. This is generally not practical for proteins because the absorbance due the acceptor would not allow excitation of the protein. Also, such high concentrations of acceptors are likely to perturb the protein structure.

Table 15.3. Approximate Concentrations for 50% Quenching in One, Two, and Three Dimensions

Equation	Concentrations for 50% energy transfer
$C_0 = (4/3\pi R_0^3)^{-1}$	9.55 x 10^{17} acceptors/cm^3 = 1.59 mM
$C_0 = (\pi R_0^2)^{-1}$	6.4 x 10^{11} acceptors/cm^2 = 4.5 x 10^{-3} acceptors/lipid
$C_0 = (2R_0)^{-1}$	5 x 10^5 acceptors/cm = 1.7 x 10^{-2} acceptors/base pair

The situation is much better in proteins and nucleic acids. In this case the acceptors need only to be about one per 222 lipids or one per 59 base pairs. This favorable situation is the result of a locally high concentration of acceptors due to their localization in the lipid or nucleic acid. The bulk concentration of acceptors can be low and is determined by the bulk concentration of membrane or nucleic acid.

A15.4. The simulations in Figure 15.31 determine the R_0 value because the two-dimensional concentration of acceptors is known from the area/lipid and the fractional acceptor concentrations. Any point on these curves can be used to calculate R_0. For an acceptor density of 0.05 and $t = \tau_D$ the value of $I_{DA}(t)/I_D^0$ is about 0.003. The value of β can be found from eq. 15.9, yielding β = 2.41. For A/PL = 0.05 the area per acceptor molecule is C_0 = 1400 Å/acceptor. Using eq. 15.10 and 15.11 yields R_0 = 39.8 Å, which agrees with the value of 40 Å given in [50].

CHAPTER 16

A16.1. A. Without experimentation, it is not possible to predict how the fluorescence properties of the protein will vary when it is unfolded. In general, one can expect the extent of tyrosine fluorescence to increase when the protein is unfolded. This could be detected by excitation at 280 nm. The tyrosine emission would appear near 308 nm. It is also probable that the fluorescent intensity or the emission maxima of the single-tryptophan residue would change as the protein is unfolded. Once the spectral characteristics of the native and unfolded states are determined, the data can be used to quantify the unfolding process. It is important to remember that anisotropy or lifetime measurements may not accurately reflect the fractional populations of the folded and unfolded states. This is particularly true if the quantum yields of the fluorescent residues in the protein change upon unfolding.

B. The extent of exposure to the aqueous phase could be studied by measuring the Stern-Volmer bimolecular quenching constant (k_q) and comparison of the measured values with those observed for an N-acetyl-L-tryptophanamide in the same solvent. One should choose the neutral tryptophan analogue to avoid electrostatic effects on the quenching process. The extent of exposure to the aqueous phase can be estimated by comparing the measured quenching constant for the protein with that found for the model compounds.

C. If the protein associates to form a dimer, it is possible that the tryptophan residue becomes shielded from the aqueous phase. In this case one can expect a change in the intensity or emission maximum of the protein. If the tryptophan residue remains exposed to the aqueous phase upon dimer formation, then it is probable that the emission spectrum and intensity will remain the same. In this case the extent of the association should still be detectable by changes in the steady-state anisotropy.

D. In order to measure the distance of the tryptophan to the reactive site it is necessary to select an appropriate acceptor and to covalently label the protein. It is critical for the protein to be completely labeled with acceptor, because the unlabeled fraction will contribute a large amount to the measured intensity, resulting in an underestimation of the distance. Following calculation of the Förster distance, R_0, from the spectral properties of the donor and acceptor, the distance can be measured from the decrease in the donor quantum yield due to the presence of acceptor.

E. While not immediately obvious, the extent of energy transfer from a tryptophan donor to an acceptor is expected to change upon association of the acceptor-labeled monomers. This is because, upon dimerization, each tryptophan residue will be brought into proximity of the acceptor on the other subunit. Hence each tryptophan will transfer to two acceptors, resulting in a higher amount of energy transfer and a lower donor quantum yield in the dimeric state.

A16.2. A. Dimerization could be detected from the steady-state intensity or the intensity decay. Upon dimer formation one will observe a twofold increase in the relative quantum yield. If the dimerization occurs due to a change in protein concentration, then it is necessary to normalize the measured intensities to the same protein concentration. If dimerization occurs as a result of a change in solution conditions, then the intensity change may be observed at a constant protein concentration.

B. Dimer formation could be detected by an increase in the mean lifetime. When dimerization is partially complete one expects the decay to be a double exponential.

C. Dimerization could not be detected from the steady-state anisotropy. The anisotropy (r) of the monomer and dimer can be calculated using the Perrin equation:

$$r = \frac{r_0}{1 + \tau/\theta} \tag{16.6}$$

where τ is the lifetime and θ is the rotational correlation time. The steady-state anisotropy of the monomer (r_M) and dimer (r_D) are equal: $r_M = r_D = 0.10$.

D. Dimerization could be detected by measuring the anisotropy decay, which will display a longer mean correlation time as dimers are formed.

E. When 50% of the monomers have formed dimers, these dimers contribute twice as much as the monomers to steady-state intensity. Hence the fractional intensities are $f_M = 0.33$ and $f_D = 0.66$. The steady-state anisotropy is given by

$$r = 0.33 r_M + 0.66 r_D = 0.10 \tag{16.7}$$

and is unchanged during dimerization.

For the intensity decay we need to calculate the values of α_M and α_D. The relative values are given by $\alpha_M = 0.33/2.5 = 0.13$ and $\alpha_D = 0.66/5.0 = 0.13$. Hence the intensity decay is given by

$$I(t) = 0.5 \exp(t/\tau_M) + 0.5 \exp(-t/\tau_D) \tag{16.8}$$

The α_i values are equivalent because we assumed that the intensities and lifetimes both increased by the same amount, meaning that the radiative decay rate stayed the same.

For a mixture of monomers and dimers the anisotropy decay follows the associated model, where each decay time is associated with one of the correlation times. At any time t the fractional intensity of the monomer or dimer is given by

$$f_M(t) = \frac{0.5e^{-t/\tau_M}}{I(t)} \tag{16.9}$$

$$f_D(t) = \frac{0.5e^{-t/\tau_D}}{I(t)} \tag{16.10}$$

where $I(t)$ is given by eq. 16.8. The anisotropy decay is given by

$$r(t) = f_M(t)r_M(t) + f_D(t)r_D(t) \tag{16.11}$$

Hence this mixture of monomers and dimers displays an associated anisotropy decay.

A16.3. There are two possible explanations for the CRABPI emission spectra in Figure 16.74. Figure 16.6 shows that the absorption spectra of indole shift to longer wavelengths with increasing solvent polarity and/or hydrogen bonding. CRABPI contains three tryptophan residues in different environments, which probably results in slightly different absorption spectra. An increase in excitation wavelength could result in selective excitation of the tryptophan residues in a more polar environment, which have longer-wavelength emission maxima.

A second possible explanation is a real-edge excitation shift (REES). A solution of indole or tryptophan in a viscous polar solution will show a shift to longer-wavelength emission as the excitation wavelength is increased. This effect is due to selective excitation of those fluorophores that are surrounded by solvent molecules that have orientations similar to the relaxed excited state. In the case of CRABPI the dominant cause of the emission spectral shifts is probably the different environments of the three tryptophan residues.

A16.4. The emission spectra in Figure 16.75 show that the region of MRP near W93 binds to calmodulin. The N-terminal region of MRP does not appear to interact with calmodulin, or at least interaction does not result in a spectral shift. The presence or absence of interaction of W4 with calmodulin could be further studied by steady-state anisotropy measurements. If W4 does not interact with calmodulin, then there should be no change in the anisotropy of W4 upon addition of calmodulin.

A16.5. Figure 16.76 shows the steady-state intensities of WT-LADH and the W314L mutant. For both acrylamide and iodide the amount of quenching is higher for W15 in the mutant protein than for the WT protein containing both W15 and W314. The Stern-Volmer plots in Figure 16.77 show a higher quenching constant for W15 in W314L than for the WT protein. The data in Figure 16.76 and 16.71 thus indicate that W15 in LADH is more accessible to water-soluble quenchers than is W314, which contributes part of the observed intensity in the WT protein. The modified Stern-

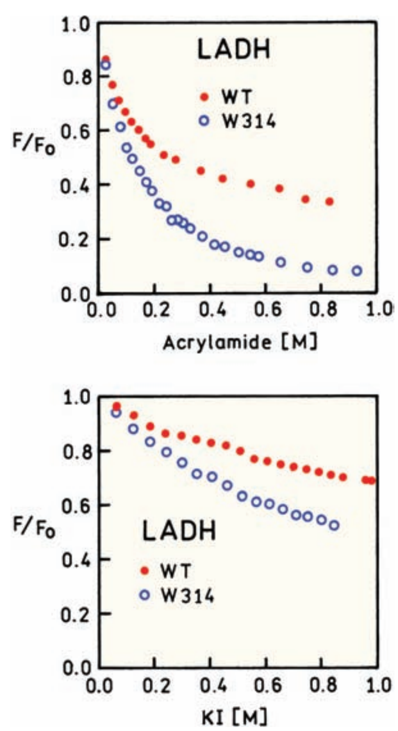

Figure 16.76. Fluorescence intensity of WT-LADH and the W314L tryptophan mutant in the presence of acrylamide and iodide. Revised from [201].

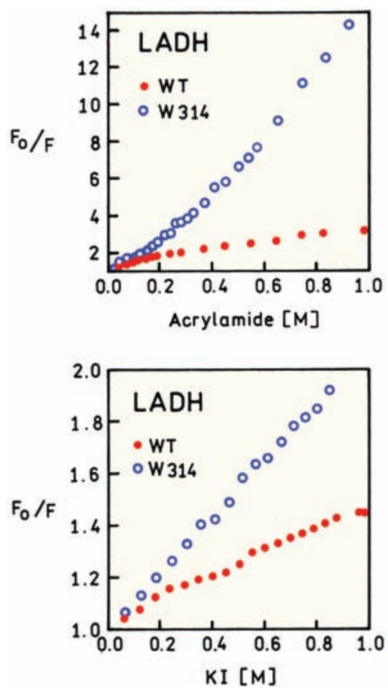

Figure 16.77. Stern-Volmer plots for acrylamide and iodide quenching of WT-LADH and the W314L tryptophan mutant.

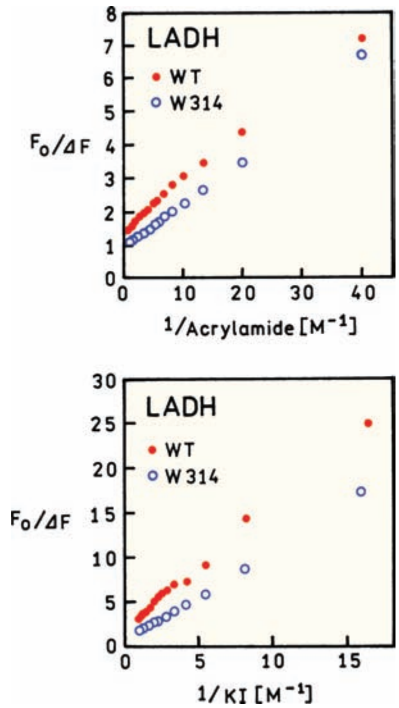

Figure 16.78. Modified Stern-Volmer plots for iodide and acrylamide quenching of WT-LADH and the W314L tryptophan mutant.

Volmer plots in Figure 16.78 suggest a somewhat higher *y*-axis intercept for the WT protein than for W314L. A higher *y*-axis intercept indicates a larger fraction of fluorescence that is not accessible to quenchers, which in the case of the WT protein is W15.

CHAPTER 17

A17.1. The activation energy for any process can be calculated by plotting the logarithm of the rate constant (k) versus the inverse of the temperature in degrees Kelvin. For an anisotropy decay the rotational rate (R) is related to the rotational correlation time (θ) by $\theta = (6R)^{-1}$. The plot of ln $(6R)$ versus $(EK)^{-1}$ is shown in Figure 17.49. The activation energy can be calculated from the Arrhenius equation:[148]

$$\ln(k) = \ln(6R) = -\frac{E_A}{R_g} + \ln A \qquad (17.4)$$

where A is a constant of integration and R_g is the gas constant. This equation is simply an expression that the rate of a process depends on a frequency factor and the energy needed to pass over an energy barrier:

$$k = A \exp^{(-E_A/RT)} \qquad (17.5)$$

From this analysis (Figure 17.49) one finds $E_A = 6.178$ kcal/mole, which is typical for rotational diffusion of proteins in water. Also, this value is comparable to the activation energy for the temperature-dependent viscosity of water, $E_A = 4.18$ kcal/mole.

The steady-state anisotropy for RNase T_1 at each temperature can be calculated from the Perrin equation

$$r = \frac{r_0}{1 + \tau/\theta} \qquad (17.6)$$

Hence the values are expected to be 0.151, 0.137, 0.128, 0.114, and 0.104, in order of increasing temperature from –1.5 to 44.4°C in Table 17.7.

A17.2. The cone angle for tryptophan rotational freedom can be calculated from the ratio of the anisotropy amplitude associated with the long correlation time, to the

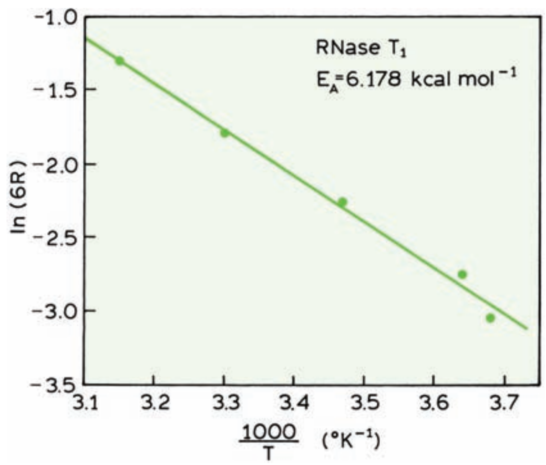

Figure 17.49. Arrhenius plot for the rotational correlation times of RNase T_1. Data from [54].

total anisotropy. The fractional contribution of the long correlation time (t_L) is given by

$$f_L = \frac{r_{01}}{r_{01} + r_{02}} \tag{17.7}$$

This fraction can be related to the displacement of the transition dipole according to the definition of anisotropy:

$$\cos^2\beta = \frac{2f_L + 1}{3} \tag{17.8}$$

Alternatively, this fraction can be related to the angle (θ_c) through which the tryptophan rotates before striking an energy barrier:

$$f_L = \left[\frac{1}{2}\cos\theta_c(1 + \cos\theta_c)\right]^2 \tag{17.9}$$

Application of these expressions to the data in Table 17.4 yields the following results in Table 17.9.

A17.3. The time-zero anisotropy, $r(0)$, for RNase T_1 in Table 17.7 is derived from the time-domain data and is lower than from other reports. One possible origin of the difference is the shorter excitation wavelength (295 nm) for the time-domain data and the possibility of a small error in the reported excitation wavelength. Another difference is that $r(0)$ was a variable parameter in the analysis of the time-domain data. It is possible that a short component in the anisotropy decay was missed by limited time resolution, as suggested by molecular dynamics simulations or RNase T_1.[149]

A17.4. A. The intensity decays more slowly at longer emission wavelengths. This indicates that the mean decay time is increasing. In this case the effect is due to an increasing fractional contribution of the long-lived component (9.8 ns).

B. The decay-associated spectra are calculated using the data in Table 17.8 and eq. 17.3, resulting in the DAS shown in Figure 17.50. In order to interpret the DAS one has to assume that each decay time (3.8 or 9.8 ns) is associated with one of the tryptophan residues. Using this assumption the 3.8 ns decay time is associated with a blue-shifted emission and a lower quantum yield than the red-shifted 9.8 ns residue.

C. The most rigorous way to confirm assignment of the DAS is to create the single tryptophan mutants. Each mutant should display one of the calculated DAS. One could also use quenching by iodide or acrylamide with the two tryptophan

Table 17.9. Angular Freedom of NATA and Tryptophan Residues in Single-Tryptophan Peptides and Proteins at 20°C

Proteins	$r_0 = r_{01} + r_{02}$	f_L	β (deg)	θ_c (deg)
RNase T_1, 20°C	0.310	1.00	0.0	0.0
Staph. nuclease	0.321	0.944	11.1	11.2
Monellin	0.315	0.768	23.2	23.8
ACTH	0.308	0.386	39.8	43.8
Gly-trp-gly	0.325	0.323	42.2	47.3
NATA	0.323	1.00	0.00	0.00
Melittin monomer	0.323	0.421	38.4	41.9
Melittin tetramer	0.326	0.638	29.4	30.8

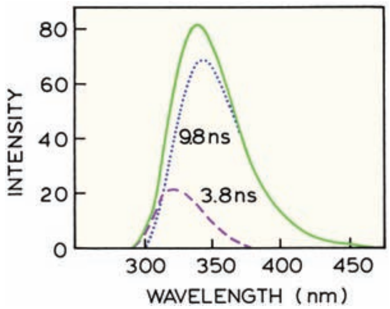

Figure 17.50. Decay-associated spectra calculated from Table 17.7. Data from [147].

wild type protein. In this case one expects the 9.8-ns emission to be more sensitive to quenching given its longer lifetime and higher exposure to the aqueous phase. The emission spectra could also be resolved by the quenching-resolved method.

A17.5. The Förster distance for any given value of κ^2 can be calculated using

$$R_0(\text{in Å}) = 9.78 \times 10^3[\kappa^2 n^{-4} Q_D J(\lambda)]^{1/6} \quad (17.10)$$

Using this expression the Förster distance is 35.1 Å for $\kappa^2 = 2/3$ and 42.2 Å for $\kappa^2 = 2$. Since the crystal structure shows $\kappa^2 = 2$, the R_0 value of 42.2 Å should be used to calculate the tryptophan-to-heme distance. This distance r can be calculated using the transfer efficiency (E) and R_0 values from

$$E = \frac{R_0^6}{R_0^6 + r^6} \quad (17.11)$$

For a transfer efficiency of 97% the distance is r = 23.6 Å using R_0 = 42.2 Å. If the value of R_0 = 35.1 Å is used, then r = 19.7 Å. The trp-to-heme distance[106] from the crystal structure is 17.2 Å. Even though the crystal structure shows $\kappa^2 = 2$, the calculated distance is in better agreement with the structure using κ^2 = 2/3.

CHAPTER 18

A18.1. The anisotropy of DPPS is higher for two-photon excitation because of $\cos^4 \theta$ photoselection. The ratio of the two- to one-photon anisotropies is near 1.39, which is close to the predicted values for parallel transitions: 1.425 (Section 18.5).

The anisotropy is independent of temperature because the lifetime decreases with increasing temperature. The decrease in lifetime offsets the decrease in correlation time, resulting in a constant anisotropy.

A18.2. The output of mode-locked dye lasers is usually cavity dumped by a device inside the laser cavity. During the time periods between dumping, power builds up in the optical cavity and the average power does not decrease much as the repetition rate is decreased. The repetition rate of a Ti:sapphire laser is usually reduced using a pulse picker that is outside the cavity. The extra pulses are discarded and there is no buildup of power in the cavity between picking. The average power drop is proportional to the decreased repetition rate. For this reason Ti:sapphire lasers are usually used without pulse pickers with an 80-MHz repetition rate. The FD data in Figure 18.17 were obtained using the harmonic content of the 80-MHz pulse train so that only a limited number of frequencies were measured (Chapter 5).

A18.3. Release of calcium in the cell results in increased energy transfer in the cameleon. When energy transfer increases the donor intensity at the shorter wavelength (480 nm) decreases relative to the acceptor intensity at 535 nm. Hence the ratio becomes larger, which is shown on the scale as the red color.

CHAPTER 19

A19.1. The lifetimes can be calculated using $\tan \phi = \omega\tau$. From Figure 19.13 the phase angles at 0 and 20.55% oxygen are 48 and 15°, respectively. Recalling the frequency $\omega = 2\pi x$, the respective lifetimes are 45.2 and 10.9 µs.

A19.2. The data in Figure 19.80 can be used to determine the lifetimes of camphorquinone in PMMA at various partial pressures of oxygen. These values can be used to construct a lifetime Stern-Volmer plot (Figure 19.83). The oxygen bimolecular quenching constant is near 2.8×10^6 M^{-1} s^{-1}, which is nearly 10^4 smaller than that for oxygen in water. This suggests a low diffusion coefficient of oxygen in PMMA of about 7×10^{-9} cm^2/s. Of course, the accuracy of these values depends on the assumed oxygen solubility in PMMA.

A19.3. Careful examination of Figure 19.9 reveals that $[Ru(Ph_2phen)_3]^{2+}$ is quenched tenfold at 30 torr oxy-

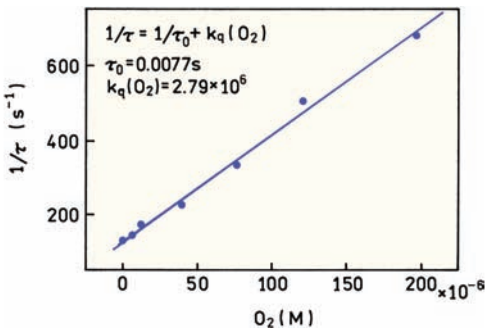

Figure 19.83. Stern-Volmer plot for oxygen quenching of camphorquinone in PMMA. Data from [308].

gen. The Stern-Volmer quenching constant is proportional to the lifetime, which is near 5 μs. Hence for the 5-ns probe $F_0/F = 1.009$ at this same oxygen pressure. At the highest oxygen pressure of 80 torr, the short-lifetime probe will be quenched less than 3%. This extent of quenching is negligible, so the 5-ns probe can serve as an intensity reference.

A19.4. The spectra in Figure 19.81 show that the absorption of TB decreases with decreasing pH. The high-pH form of TB is the acceptor for SR101. As the percentage of CO_2 increases the pH of the polymer matrix decreases. This results in a decreased absorbance of TB, less RET from SR101 to TB, and an increase in the apparent lifetime. The increases in apparent lifetime result in the larger phase angle with 2% CO_2. The apparent lifetimes of 0 and 2% CO_2 are 0.35 and 1.24 ns, respectively.

A19.5. A. The range of anisotropies can be calculated from the Perrin equation

$$r = \frac{r_0}{1 + (\tau/\theta)} \tag{19.15}$$

The anisotropy of the free peptide will be 0.080, and the anisotropy of Ab-Fl-P will be 0.385.

B. The anisotropies are additive (e.g., 19.14). Hence the anisotropy with 10% free Fl-P is given by

$$r = 0.10(0.08) + 0.90(0.385) = 0.355 \tag{19.16}$$

C. Displacement of Fl-P from Rh-Ab will result in a tenfold increase in the intensity of Fl-P due to elimination of RET. For such cases, the fractional intensity of the free and bound forms are given by

$$f_F = \frac{m_F q_F}{m_F q_F + m_B q_B} \tag{19.17}$$

$$f_B = \frac{m_B q_B}{m_F q_F + m_B q_B} \tag{19.18}$$

where m_i are the molecular fractions in the free or bound state, and q_i are the quantum yields. If $q_F = 10q_B$, then

$$f_F = \frac{10m_F}{10m_F + m_B} \tag{19.19}$$

For a molecular fraction of 10%, $f_F = 0.53$. Hence 10% displacement of Fl-P results in over 50% of the emission from the free peptide. The anisotropy is

$$r = 0.53(0.08) + 0.47(0.40) = 0.230 \tag{19.20}$$

and is seen to decrease more rapidly with displacement of Fl-P. We used 0.40 for the anisotropy of the bound form because RET will decrease the lifetime of the fluorescein to 0.40 ns.

CHAPTER 20

A20.1. A. The decay time can be calculated from the slope of the long-lifetime component using any two points. For instance, extrapolating the long decay time to zero, the intensities of this component at $t = 0$ and $t = 500$ ns in Figure 20.50 are near 2000 and 600, respectively. For a single-exponential decay the intensities at two points in time are related by $\ln I(t_1) - \ln I(t_2) = -t_1/\tau + t_2/\tau$. Insertion of the values at $t = 0$ and $t = 500$ ns yields $\tau = 415$ ns.

B. $\alpha_1 = 0.962$, $\alpha_2 = 0.038$. These values are from Figure 20.50, following normalization of α_1 and $\alpha_2 = 1.0$.

C. $f_1 = 0.296$, $f_2 = 0.704$.

D. f_1 = 0.0004, f_2 = 0.9996. This result shows that off-gating essentially eliminates the short-lived component, decreasing its fractional contribution from 0.296 to 0.0004.

A20.2. The oxygen bimolecular quenching constant can be calculated using the decay times in the absence and in the presence of 100% oxygen. The value of $\tau_0/\tau = 16.3 = 1 + k_q\tau_0[O_2]$. Using $[O_2]$ = 0.001275 M and τ_0 = 3.7 µs one obtains $k_q = 3.24 \times 10^9\ M^{-1}\ s^{-1}$. This value is reasonably close to the diffusion-controlled limit and indicates that the quenching by oxygen is highly efficient.

CHAPTER 21

A21.1. To answer this question we need to design quenching or anisotropy measurements that could potentially be used for sequencing. Consider sequencing with four fluorescent ddNTPs. The Stern-Volmer quenching constants could be different due to either different lifetimes or different accessibilities to the collisional quencher. Then the sequence could be determined by the quenching constant for each fluorescent band on the gel. Determination of the quenching constant requires a minimum of two intensity measurements: in the absence of quencher and in the presence of a known concentration of quencher. Although such measurements are possible, the use of two samples to measure a single base is too complicated for large-scale sequencing of DNA.

Suppose that the sequencing reaction is performed with a single fluorescent primer. Because anisotropy measurements depend on molecular weight, in principle each oligonucleotide will display a different anisotropy. In practice the anisotropies for DNA oligomers, differing by a single base pair, are likely to be too similar in magnitude for useful distinction between oligomers. If the adjacent base pair changes the lifetime of the labeled oligomer, then the anisotropy measurements may be able to identify the base.

Consider the use of four fluorescent ddNTPs, each with a different lifetime. In this case the anisotropy would be different for each base pair, and the anisotropy measurement could be used to identify the base. This approach is more likely to succeed for longer oligomers, where the anisotropy will become mostly independent of molecular weight. For shorter oligomers the anisotropy will depend on the fragment length.

CHAPTER 22

A22.1. In Figure 22.15 it is clear that the F-actin is red and the green color is where the mitochondria are expected to be localized. In Figure 22.19 the colors are reversed: F-actin is green and mitochondria are red. At first glance it appears that the legend for one of the figures is incorrect, or that the cells in Figure 22.15 were labeled with fluorophores that stained actin red and mitochondria green. The legends are correct. Both images are created using pseudocolors. Figure 22.19 was created by an overlay of three intensity images. The color of each image was assigned to be similar to the emission maxima of the probes: DAPI is blue, Bodipy-FL is green, and MitoTracker is red. These assignments give the impression that Figure 22.19 is a real color image. In Figure 22.15 the colors were assigned according to lifetime. The lifetime in the nucleus was assigned a blue color, which agrees with Figure 22.19. However, in Figure 22.15 the lifetime of F-actin was assigned to be red, and the lifetime of MitoTracker was assigned to be green. The pseudocolor assignments of the red- and green-emitting fluorophores are opposite in Figures 22.15 and 22.19.

CHAPTER 23

A23.1. The intensity needed to excite the fluorophore can be calculated using eq. 23.5. If there is no intersystem crossing than $S_1 = \tau\sigma\ I_e\ S_T$. The intensity required is given by $S_1/S_T = 0.5\ \tau\sigma\ I_e$. The cross-section for absorption can be calculated using eq 23.1, yielding $\sigma = 4 \times 10^{-16} = 4$ Å^2. In performing this calculation it is important to use a conversion factor of 10^3 cm^2/liter.

The number of photons per cm^2 per second can be calculated from $I_e = 0.5\ (\tau\sigma)^{-1} = 3.1 \times 10^{23}$/cm^2 s. The power can be calculated from the number of photons per second per cm^2 and the energy per photon = $h\nu/\lambda$, yielding 103 kW/cm^2, and an area of 1 µm^2 = 10^{-8} cm^2, so the power needed to saturate the fluorophore is 0.001 watts/cm^2.

CHAPTER 24

A24.1. Figure 24.8 gives the concentration of R6G and the inverses of the $\tau = 0$ intercept give the apparent number of fluorophores. Using $G(0) = 0.12$ at 1.25 nM yields $N = 8.3$ molecules. The volume can be calculated from

$$V_{eff} = N/\overline{C}N_A$$

where N_A is Avogadro's number, yielding $V_{eff} = 11.0$ fl. The effective volume is related to the dimensions by $V_{eff} = \pi^{3/2}\, s^2 u$, which becomes $V_{eff} = 4\pi^{3/2}\, s^3$ for the assumed u/s ratio. Recalling that 10^3 liters = 1 cubic meter, one finds $s = 0.79$ µm and $u = 3.16$ µm.

A24.2. The ratio of the diffusion times can be read off the graph. Taking the maximum difference near $G(\tau) = 0.35$, one finds $\tau_D(\text{GroEL})/\tau_D(\alpha\text{-LA}) = 0.4/0.15 = 2.7$, which indicates a $3^3 = 19.7$-fold increase in molecular weight. This is somewhat less than the expected value of 49.4 from the ratio of the molecular weight. One possible explanation is the diffusion coefficient of denatured α-LA is lower than for the native protein, causing the τ_D ratio to be lower than expected.

24.3. If we know the diffusion coefficient the time can be calculated without knowing the beam diameter. The time required to diffuse 10 µm can be calculated using $\Delta x^2 = 2\Delta\tau$, where Δx is the distance. Using $D = 3 \times 10^{-8}$ cm²/s and recalling that 10^4 cm² = 1 m², one finds $\tau = 16.7$ s. The time required to diffuse 10 µm does not depend on the beam diameter, so τ is the same for a 1- or 2-µm diameter beam.

A24.4. The autocorrelation function yields the relaxation time for the opening–closing reaction, which is $\tau_R = (k_1 + k_2)^{-1}$. The equilibrium constant is given by $K = k_1/k_2$. The values of K can be determined by examining the fluorescence intensity of the beacon as a function of temperature. The fractional intensity between the low- and high-temperature intensities yields the fraction of the beacon that is open at the temperature used to collect $G(\tau)$. This fraction yields the equilibrium constant K, allowing k_1 and k_2 to be calculated.

A24.5. The volume in the TIR FCS experiment can be estimated using $V = \pi s^2 d$. The volume is 1.96 fl. The concentration needed is given by

$$\overline{C} = N/VN_A$$

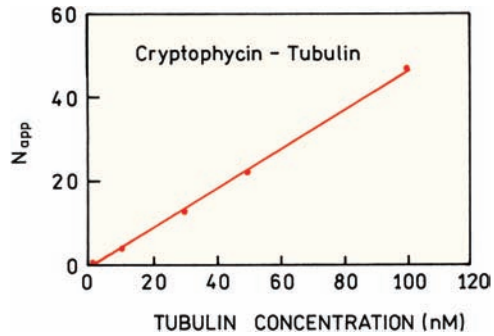

Figure 24.51. Effect of sample dilution on the apparent number of diffusing tubulin particles. Revised and reprinted with permission from [38]. Copyright © 2003, American Chemical Society.

where N_A is Avogadro's number, and

$$\overline{C} = 8.5 \text{ nM}$$

The area occupied by a single lipid molecule is 0.7 nm². The area of the illuminated membrane is 19.6 µm² = 19.6 x 10^6 nm². Hence to obtain 10 fluorophores in the illuminated area the fraction of labeled fluorophores should be 7.3 x 10^{-7}, or approximately 1 labeled lipid per 1,372,000 unlabeled lipid molecules.

A24.6. The effect of dilution on the self-association of tubulin can be determined in two ways. If the tubulin complex dissociates upon dilution then the diffusion coefficient will decrease and the autocorrelation curves shift to shorter times. Because of the change in amplitude the presence or absence of a shift cannot be seen in Figure 24.50.

Another way to determine if the complex dissociates is from the apparent number of diffusing molecules. If all the substrates are labeled, dissociation will result in a higher value of N_{app}. Figure 24.51 shows a plot of N_{app} versus total tubulin concentration. N_{app} scales linearly with concentration, showing the complexes do not dissociate. This approach is only valid if all the tubulin is labeled. If there was only one labeled tubulin per complex then dissociation would not increase N_{app} but the diffusion coefficient would change.

CHAPTER 25

A25.1. The radiative decay rate in the absence of SIF can be calculated from the quantum yield and natural lifetime

τ_N. Since $\Gamma = \tau_N^{-1}$, then $\Gamma = 2.5 \times 10^8\ s^{-1}$. Using the definition of the quantum yield in eq. 25.1 the non-radiative decay rate is given by

$$k_{nr} = \frac{\Gamma - Q_O \Gamma}{Q_O} = 122.5 \times 10^8\ s^{-1} \quad (25.5)$$

This value of k_{nr} is reasonable because k_{nr} must be significantly larger than Γ to account for the low value of $Q_O = 0.02$.

In the presence of SIF the quantum yield increases 4.8-fold to $Q_m = 0.096$. This quantum yield is related to the total decay rate by

$$Q_m = \frac{\Gamma_T}{\Gamma_T + k_{nr}} \quad (25.6)$$

so that

$$\Gamma_T = \frac{Q_m k_{nr}}{1 - Q_m} = 1.3 \times 10^9\ s^{-1} \quad (25.7)$$

The radiative decay rate due to the metal is given by $\Gamma_m = \Gamma_T - \Gamma = 1.05 \times 10^9$ s. Hence $\Gamma_m/\Gamma = 4.7$.

If only 10% of the Rose Bengal is affected, then the apparent quantum yield (Q_A) is related to the quantum yield near the SIF and in solution as

$$Q_A = 0.90 Q_O + 0.10 Q_m \quad (25.8)$$

Using $Q_A = 0.096$, then $Q_m = 0.78$. The value of Γ_T can be calculated from eq. 25.7, so that $\Gamma_T = 4.34 \times 10^{10}\ s^{-1}$, and then $\Gamma_m = 4.32 \times 10^{10}\ s^{-1}$. If only 10% of the RB population is affected by the SIF, then $\Gamma_m/\Gamma = 173$.

Index

A

B

C

D

E

F

G

J

K

L

M

N

O

P

Q

R

T

U

V

W

X

Y

Z